NSK Technical Journal

Motion & Control

No. 9

October 2000

NSK

ISSN1342-3630

MOTION & CONTROL No. 9
NSK Technical Journal
Printed and Published: October 2000
ISSN1342-3630
Publisher: NSK Ltd., Ohsaki, Shinagawa, Tokyo, JAPAN
Public Relations Department
TEL +81-3-3779-7051
FAX +81-3-3779-7431
Editor: Kyozaburo FURUMURA
Managing Editor: Yasuhiko MORITA
Design, Typesetting & Printing: Fuji Ad. Systems Corp.

Cover photos: NSK STEERING SYSTEMS EUROPE LTD. (U.K.)
NSK ISKRA S.A. (Poland)
Liberty Plant, NSK CORPORATION (U.S.A.)

NSK Technical Journal
Motion & Control
No. 9
October 2000

NSK

Contents

EA Spherical Roller Bearings

Akiyoshi Honda, Akio Miyasaka and Masahide Matsubara
Bearing Technology Center

1. Introduction

Owing to their high load capacity, self-aligning capability and easy-handling unseparable design, spherical roller bearings are widely used in steel mills, paper mills, construction equipment, industrial gearboxes, plummer blocks and material-handling and wood-processing equipment. Throughout this wide range of applications and operating environments, these bearings must provide high toughness as well as excellent rotational performance.

NSK's spherical roller bearing lineup has included the standard CD Series with pressed steel cages and high-capacity H Series with plastic cages. Recently, NSK developed EA spherical roller bearings with high-accuracy pressed steel cages (Fig. 1). The new standard for next-generation spherical roller bearings, the EA Series features high load capacity, long life, low temperature rise, high-speed capability and low noise and vibration. This report presents the design and features of EA spherical roller bearings.

2. EA Series Design Concept

To develop an improved spherical roller bearing, we began with market research to get a clear understanding of user needs and required bearing functions. We found that users regarded spherical roller bearings as general-purpose bearings that should offer high load capacity, long life, low temperature rise, high limiting speed, low vibration and noise, and toughness to endure shocks, vibration and insufficient lubrication. Also, users wanted bearings that were subject to fewer restrictions on operating temperature and lubricant type.

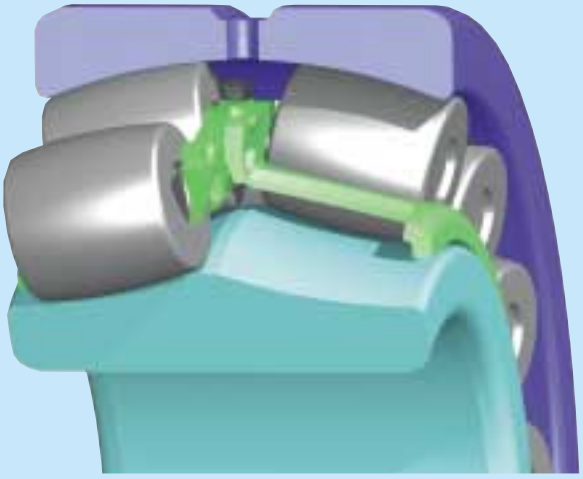

Fig. 1 EA spherical roller bearing

The internal structure of EA bearings was designed to meet the needs defined in the market research. Now we discuss the concepts behind the EA Series design. Fig. 2 compares the features of the EA Series with those of the CD Series. In order to minimize the temperature rise of spherical roller bearings, it is essential to keep the rotating rollers in a stable condition and control roller skew. In the CD Series, a guide ring performs this function (Fig. 2). By contrast, in the EA Series, the guide ring is eliminated and roller position is controlled by the cage, freeing space in the bearing interior for more and larger rollers. Additionally, the cage is double-flanged to provide

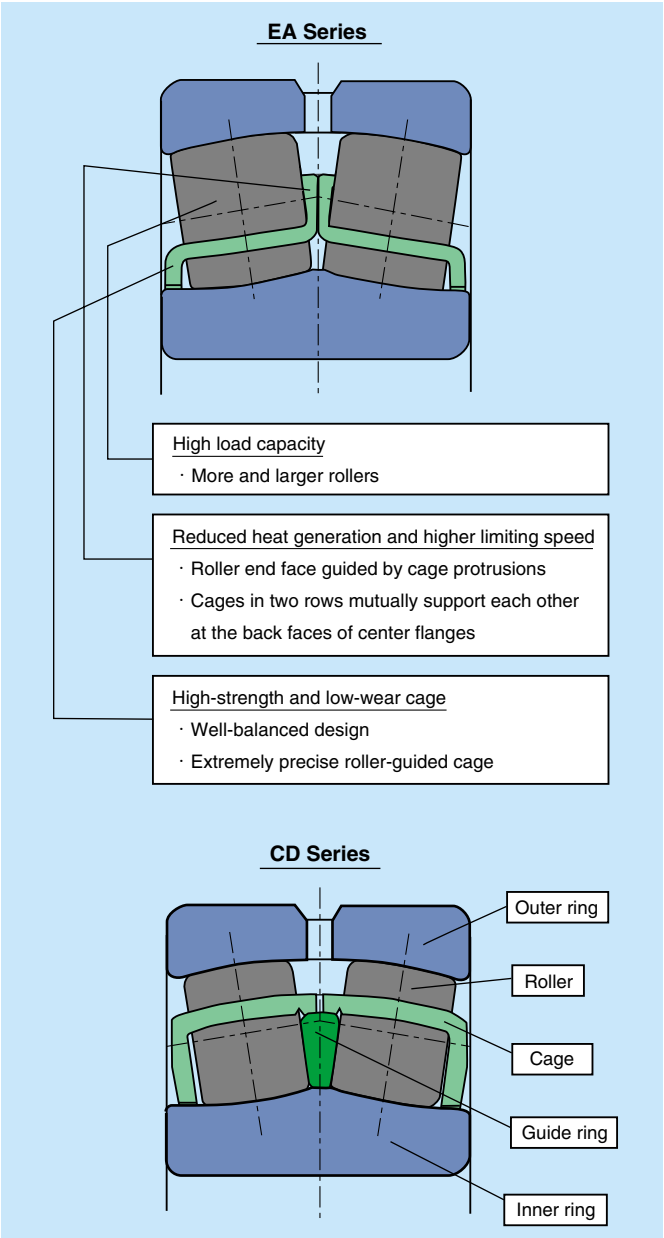

Fig. 2 Comparison of EA and CD bearing designs

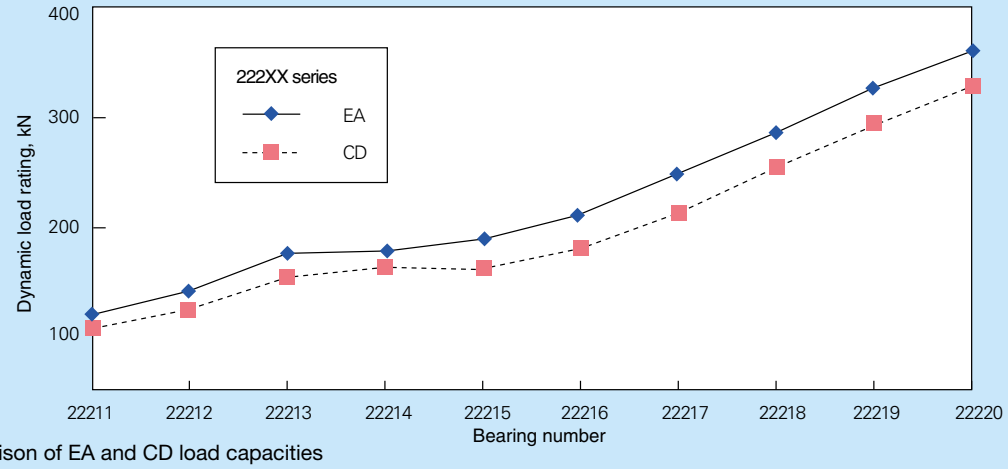

Fig. 3 Comparison of EA and CD load capacities

better structural balance. The cage flanges in the middle of the bearing have protrusions that guide the end faces of the rollers, while the back face of the flanges provides support to the cage halves mutually. Thus, the cage and rollers are kept in proper position during operation.

3. Features of EA Series

The EA Series was developed through advanced analysis techniques and harsh evaluation tests and experiments. The outstanding features of the new series are discussed in the following sections.

3.1 Higher load capacity and longer life

In the EA Series, not only does the space made available by eliminating the guide ring contribute to more and larger rollers, but also to the optimum design of the outer and inner rings. As a result, the load capacity of the EA Series is 10 to 20 percent higher than the CD Series (Fig. 3). Fig. 4 presents test results that illustrate the longer life brought about by the higher load capacity of the EA Series.

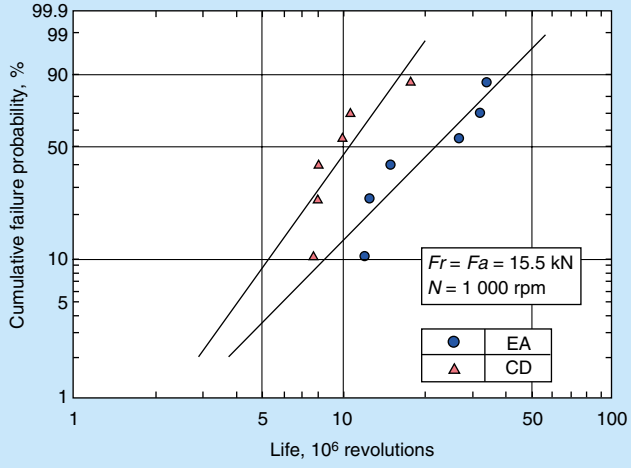

Fig. 4 Life test results

Test bearing
22211

Test conditions
Running speed: 2 000 rpm
Radial load: F_r = 12.21 kN
Axial load: F_a = 0 kN
Lubrication: Forced oil circulation
Lubricant: Terrace oil C (ISO VG10)

Test method
Gap sensors are placed close to the outer end faces of the rollers and the skew of the rollers is measured. Each of the sensors analyzes passing rollers to obtain maximum, minimum and average values of skew.

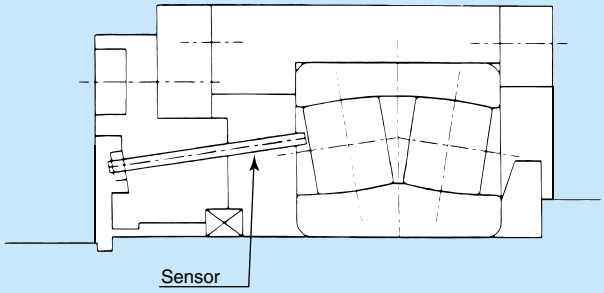

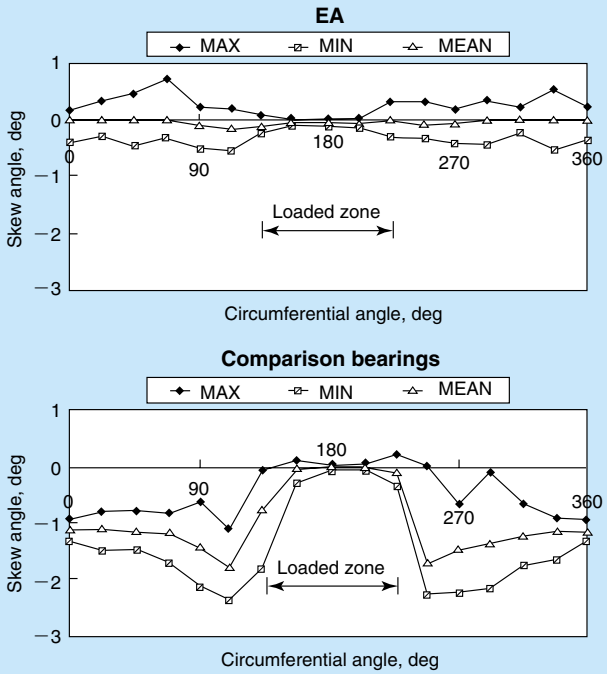

Fig. 5 Roller skew in spherical roller bearings

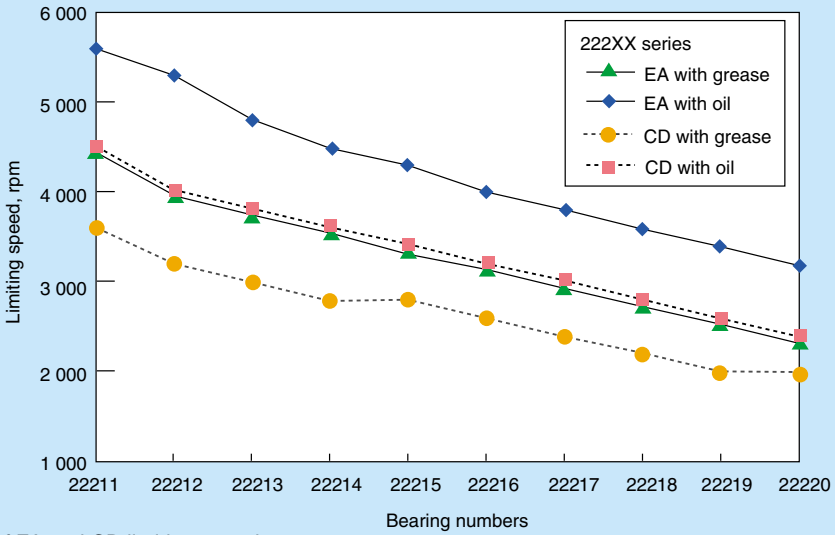

Fig. 6 Comparison of EA and CD limiting speeds

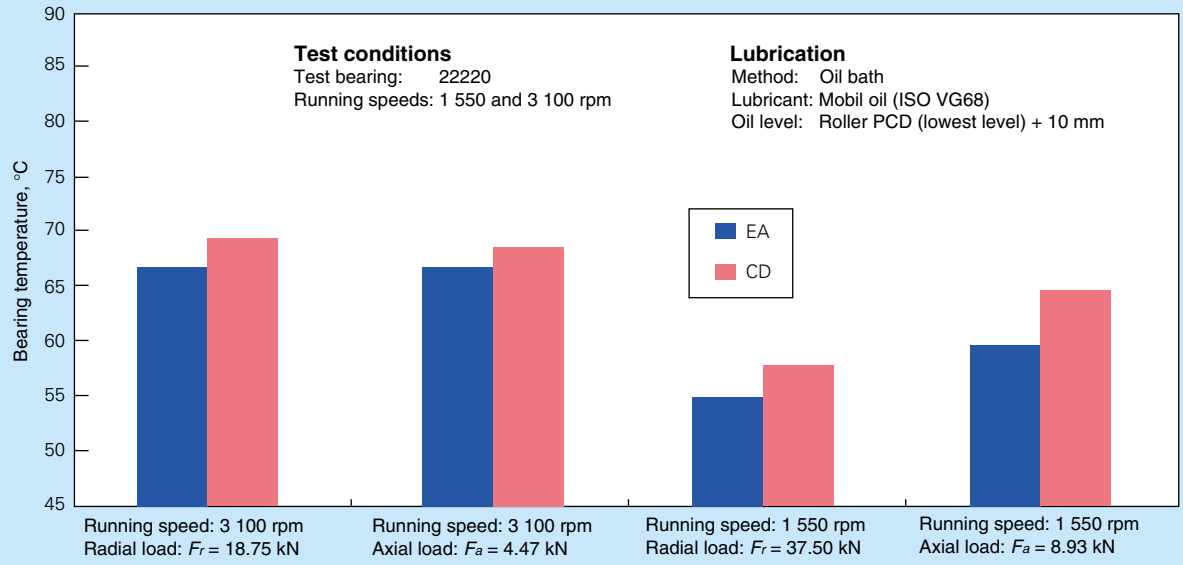

Fig. 7 Comparison of EA and CD bearing temperatures

3.2 Reduced temperature rise and higher limiting speed

Small knob-like protrusions on the center cage flange guide each roller end face and keep the rollers in the proper position. There are two such protrusions for each roller. Through accurate control of the clearance between the protrusions and the roller end faces, it is possible to achieve better roller control and minimize roller skew, without employing a guide ring. (Roller skew is the deviation of the rotational axis of a roller away from its proper axis of rotation. Generally, increasing roller skew means more sliding between the rollers and raceways and increased heat generation.) The development of highly precise cage pressing technology has ensured that the proper clearance between the protrusions and the roller end faces can be achieved on a mass-production scale.

Fig. 5 shows measurements of the roller skew of EA bearings and comparison bearings. The comparison bearings had pressed steel cages with flanges and no skew control characteristic. Like the EA bearings, they had no guide ring. As shown in Fig. 5, the rollers in the comparison bearings showed significant skewing in the non-loaded zone, while the EA bearing rollers showed much less skewing throughout the circumference of the bearing, clearly demonstrating the skew-controlling effect of the cage.

The low temperature rise of EA bearings is achieved not only through the cage's effective control of roller attitude but also the design optimization of the raceways and roller contact surface geometry. NSK's proprietary "bearing performance analysis software" was used to review and compare different combinations of bearing specifications to determine the optimum design.[1)]

While increasing the length and number of rollers generally causes greater temperature rise during rotation,

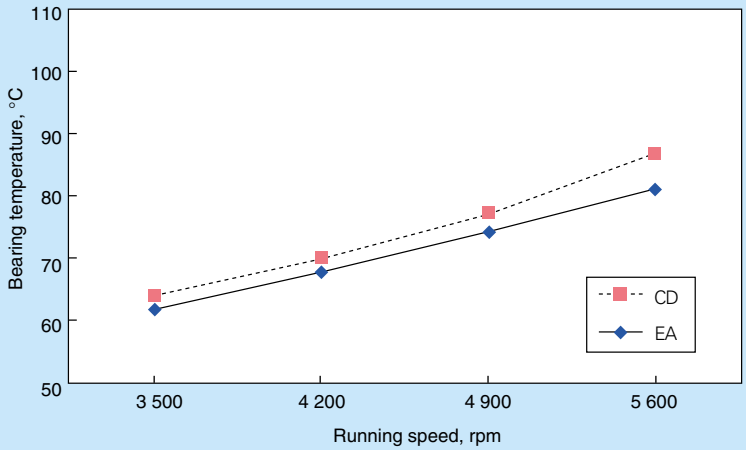

Test conditions

Test bearing: 22220 (100 × 180 × 46 mm)
Running speeds: 3 500, 4 200, 4 900 and 5 600 rpm
Load: Radial load of F_r = 19.4 kN
Lubrication
Method: Forced oil circulation
Lubricant: Mobil oil (ISO VG68)
Oil flow rate: 1 liter/min (at constant oil temp. of 40°C)

Note: This test was performed at speeds exceeding the limiting speed.

Fig. 8 High-speed test of bearing 22220

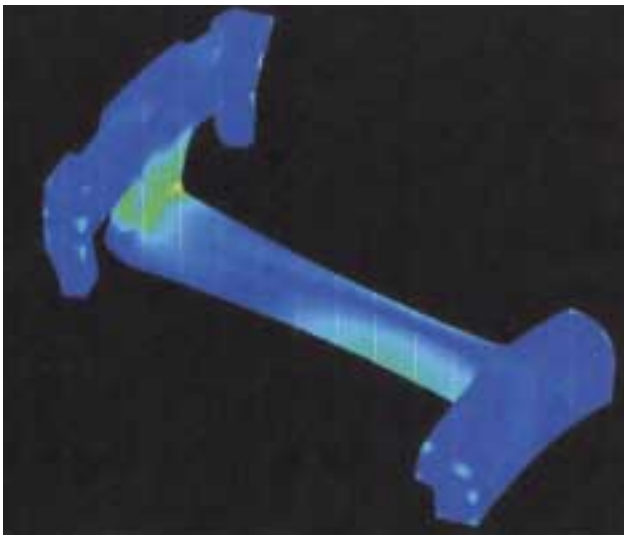

Fig. 9 FEM analysis of cage

with the special measures described above, EA bearings have lower temperature rise and significantly higher limiting speed than the CD Series. Fig. 6 compares the limiting speeds of the EA and CD Series. Fig. 7 shows the results of temperature rise tests of 22220 EA and CD bearings. EA and CD bearings were also tested at speeds exceeding their limiting speed under forced oil lubrication. The test results are shown for reference in Fig. 8.

3.3 High-strength and low-wear cage

In contrast to the CD Series' single-flange cage that is guided by the inner ring, the EA Series cage has two flanges and is guided by the rollers, as shown in Fig. 2. By eliminating the guide ring, the EA design ensures good balance of the cage. To ensure that impact loads were evenly dispersed and thus minimize the maximum stress level of the cage, the finite element method (FEM) was used in its design to analyze the forces acting between the cage and rollers and optimize both the cage dimensions

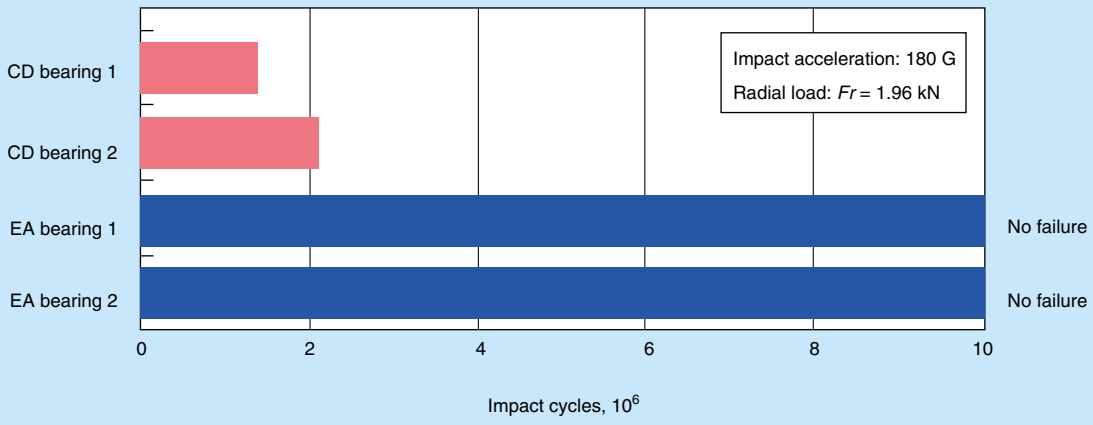

Fig. 10 Drop impact test of 22211

Test conditions

Test bearing:
22218 (90 × 160 × 40 mm)
Running speeds:
3 900, 5 070 and 6 240 rpm
Loads:
Radial load F_r = 14.6 kN (for 2 hrs. at each running speed)
Axial load F_a = 2.48 kN (for 2 hrs. at each running speed)
Lubrication:
Method: Forced oil circulation
Lubricant: Mobil oil (ISO VG68)
Oil flow rate: 1 liter/min. (at constant temp. of 40°C)
Time tested:
12 hours

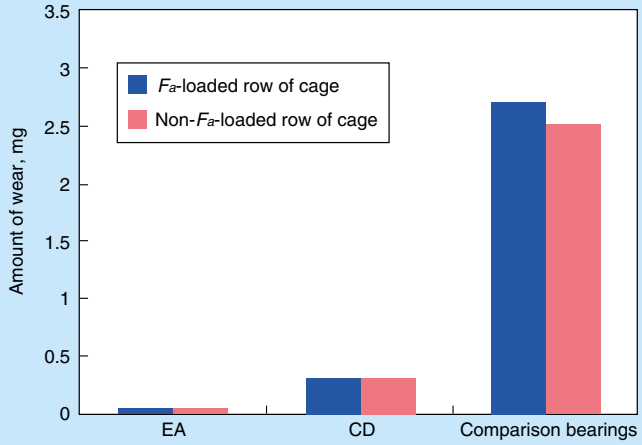

Fig. 11 Comparison of cage wear

Test conditions

Test bearing:
22211 (55 × 100 × 25 mm)
Running speed:
3 000 rpm
Load:
Radial load F_r = 5.98 kN
Lubrication:
0.05 milliliters of oil injected using a microsyringe
Evaluation:
Time from start of test until sharp rise in torque

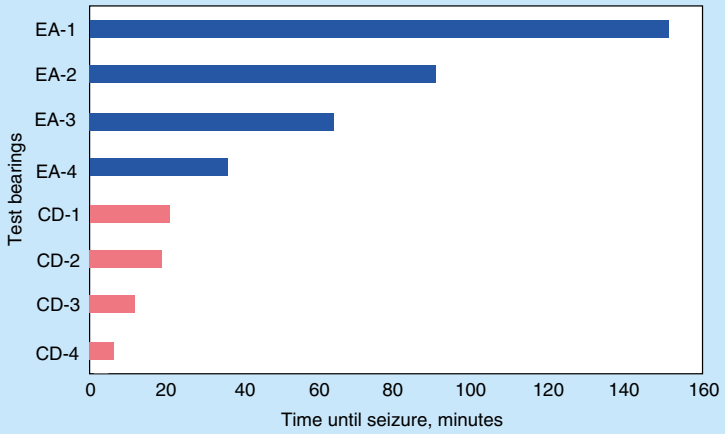

Fig. 12 Seizure test

and the cage riding clearance. Fig. 9 shows an image from FEM analysis. The EA cage has remarkably improved strength, ensuring greater bearing reliability in applications where shocks and vibration are common. Fig. 10 compares dropping impact resistance of radially loaded EA and CD Series test bearings. To accelerate evaluation in this test, the impact velocity was far greater than in actual service.

The new EA cage is guided by the rollers and eliminates wear caused by sliding between the rollers and inner ring raceway. In addition, improved press-forming technology greatly enhanced the dimensional accuracy of the cage, greatly reducing wear under severe operating conditions. Fig. 11 compares the cage wear of EA, CD and the previously mentioned comparison bearings tested at a speed higher than the limiting speed. The amounts of cage wear shown in Fig. 11 were determined by weighing the cages before and after the test. Clearly, the EA cages demonstrated the lowest wear.

3.4 High seizure resistance

To assess seizure resistance under lubricant-starved conditions, the time to seizure of bearings operated while lubricated with only a very small amount of oil was measured. Fig. 12 compares results on the EA and CD Series bearings. Clearly, EA bearings have higher seizure resistance than CD bearings. This outstanding seizure resistance stems from the previously discussed low heat-generating property of EA bearings.

3.5 Low vibration and low noise

Figs. 13 and 14 compare the vibration and noise levels of EA and CD bearings. Owing to their improved cage accuracy, which enables better control of the clearance between the cage and rollers, EA bearings generate less vibration and noise than CD bearings.

3.6 Higher permissible operating temperature

Both the outer and inner rings of EA Series bearings undergo heat treatment to ensure dimensional stability under high operating temperatures. This, coupled with the use of pressed steel cages, enables operation at temperatures up to 200°C (392°F).

Test conditions

Test bearing:
22218 (90 × 160 × 40 mm)
Running speeds:
6 100, 7 950 and 9 800 rpm
Load:
Radial load F_r = 9.85 kN
Lubrication:
Method: Forced oil circulation
Lubricant: Mobil oil (ISO VG68)
Oil flow rate: 1 liter/min (at constant temp. of 40°C)

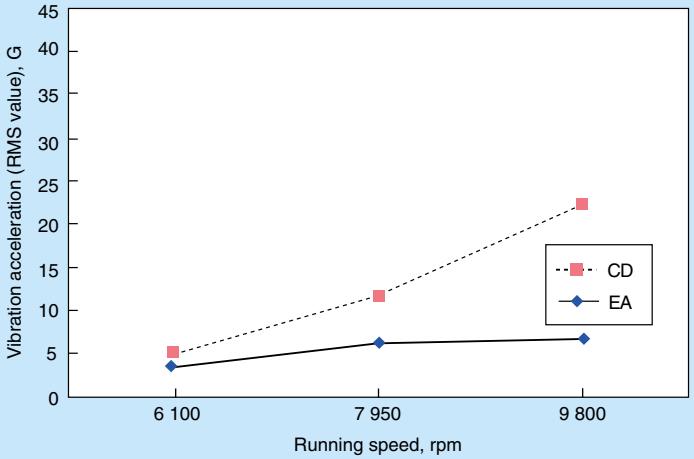

Fig. 13 Comparison of vibration

Measurement conditions

Running speed:
1 000 rpm
Radial load:
F_r = 1.47 kN
Lubricant:
ISO VG68
Measurement:
Data obtained 5 minutes after start of bearing rotation with a microphone positioned 250 mm from the center of the test bearing

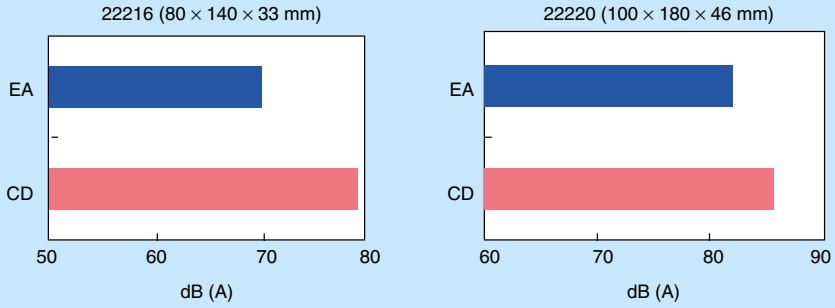

Fig. 14 Comparison of noise levels

4. Conclusion

With their innovative, advanced design and highly precise pressed steel cages, EA Series bearings offer longer life; higher limiting speed; greater load capacity, seizure resistance and toughness; and reduced heat generation, vibration and noise. They are designed for easier handling and can operate at temperatures up to 200°C (392°F). The EA Series so far includes bearing numbers 22210–26, 22310–26 and 21309–18. This range will be expanded in line with the position of the EA Series as NSK's core spherical roller bearing product.

Reference:

1) Hirotoshi Aramaki, NSK Technical Journal No. 663, (1997) 1–7. [in Japanese]


Akiyoshi Honda


Akio Miyasaka


Masahide Matsubara

ROBUST Series High-Speed Precision Angular Contact Ball Bearings for Machine Tool Spindles

Yukio Ohura
Bearing Technology Center
Yoshiaki Katsuno and Sumio Sugita
Research and Development Center

1. Introduction

Concerns about global warming and other environmental problems are taking on greater importance in many industries as well as in society as a whole. In line with this trend, machine tools, which are used to produce parts for automobiles, home appliances, office automation equipment and other products, are required to operate at higher levels of productivity and workability while saving energy and reducing their environmental impact. Essentially, to meet these requirements, tool and spindle speed must be increased while energy consumption is reduced. In this report, we first discuss the latest trends in machine tools, with reference to the machines displayed at the 19th Japan International Machine Tool Fair (JIMTOF) held in October 1998, and then present NSK's ROBUST Series of high-speed precision angular contact ball bearings for the machine tools of the 21st century.

2. Trends toward Higher-Speed Machine Tools at JIMTOF '98

The theme of JIMTOF '98 was "Challenges for the 21st Century" and various types of environmentally friendly and state-of-the-art machines were exhibited. These machines were capable of performing complex, automated and parallel-mechanism machining at high speeds with

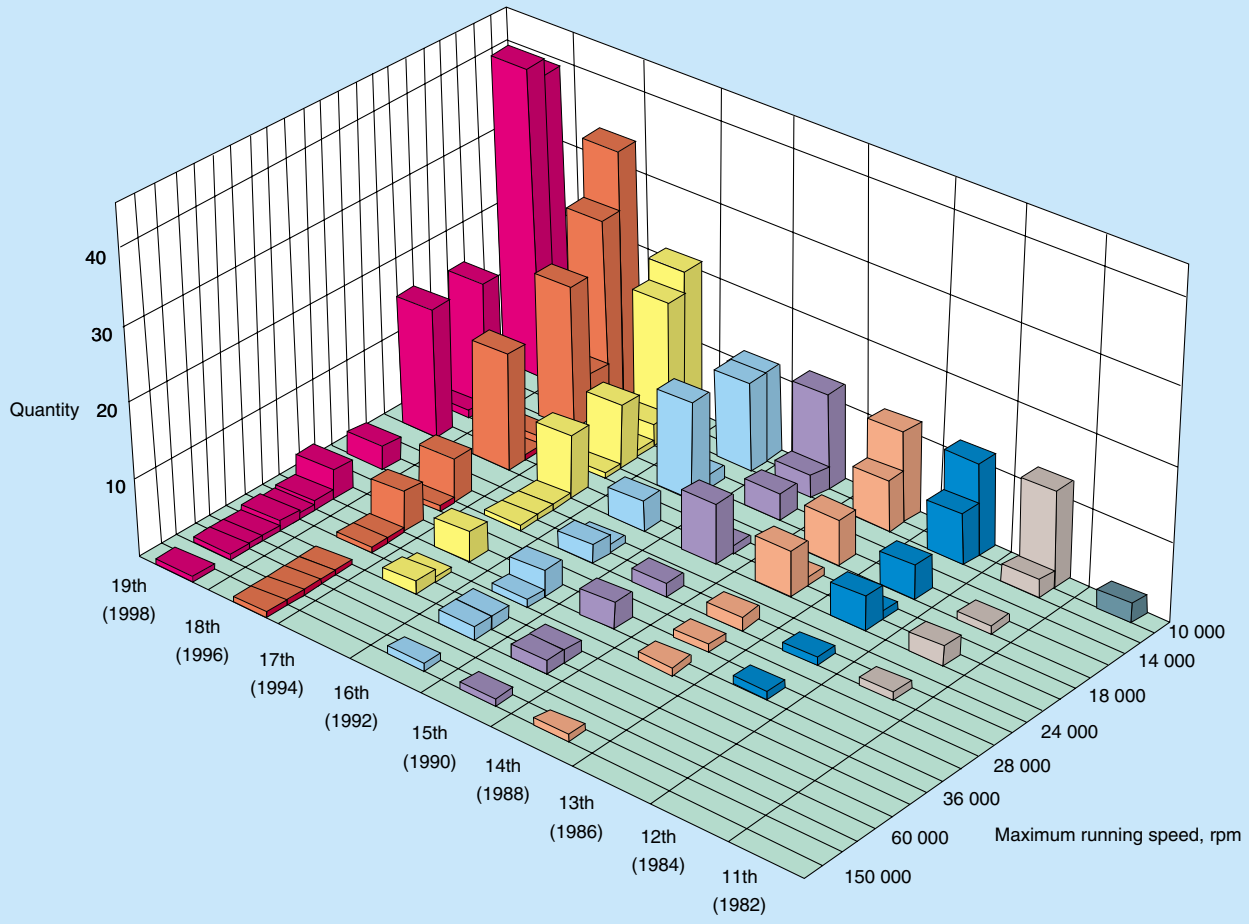

Fig. 1 Numbers of machine tools with maximum speeds of 10 000 rpm or higher exhibited at Japan International Machine Tool Fairs from 1982 to 1998

		19th (1998)	18th (1996)	17th (1994)	16th (1992)	15th (1990)	14th (1988)
Machines with 600 000 $d_m n$ or higher		166	142	90	72	49	42
Grease lubrication	Total	62	44	27	20	17	12
	Ceramic balls*	26	24	12	10	8	2
Oil-air lubrication	Total	62	49	41	32	25	24
	Ceramic balls*	43	26	30	23	15	13
Oil mist lubrication	Total	29	16	8	5	1	1
	Ceramic balls*	20	9	6	4	0	0
Oil jet lubrication	Total	2	2	2	3	3	3
	Ceramic balls*	1	0	2	0	0	0
Under-race jet lubrication	Total	7	7	3	3	0	0
	Ceramic balls*	5	7	0	3	0	0
Unknown and others	Total	4	24	9	9	3	2
	Ceramic balls*	3	2				

* Machines using hybrid ceramic angular contact ball bearings

Fig. 2 Numbers of machining centers capable of 600 000 $d_m n$ or higher exhibited at Japan International Machine Tool Fairs from 1988 to 1998

great precision. In the following sections, we describe the trends in machine tools spindles toward higher speed and rigidity to meet the ever-increasing requirements for higher efficiency. We do this by comparing the machine tool spindles exhibited at the '98 JIMTOF with those from fairs in preceding years.

2.1 Spindles exhibited from 1982–1998

Fig. 1 shows the total number of machine tool spindles capable of running speeds higher than 10 000 rpm exhibited at JIMTOF from 1982 to 1998. The number of machine tool spindles displayed at JIMTOF '98 exceeded 140, up 15% over the preceding fair. Spindles capable of speeds greater than 10 000 rpm were first exhibited at the 11th fair in 1982 and increasing numbers of such spindles have been displayed since then. The 12 000-rpm spindles exhibited at JIMTOF '98 (40 units) were nearly double those at JIMTOF '96. Approximately 75 percent of those 12 000-rpm spindles were for tool sizes of NT40 and NT50 or equivalents, and their diameters were mostly 80 and 100 mm, respectively. This illustrates a trend toward increasing spindle diameter to achieve greater rigidity in a wider speed range. One noticeable characteristic of general machine tool design at JIMTOF '98 is five-plane machining capability combined with bed swinging and turning mechanisms. Additionally, some of the machines exhibited were designed to eliminate setup changes to achieve higher efficiency.

2.2 Lubrication methods and bearing specifications

Fig. 2 lists the lubrication methods and the number of the exhibited machining centers with spindles using hybrid ceramic angular contact ball bearings, whose rolling elements are made of Si_3N_4 (silicon nitride) and whose $d_m n$ (pitch circle diameter of rolling elements, d_m (mm) × running speed, n (rpm)) values are 600 000 or greater. A total of 166 such machining centers were exhibited at JIMTOF '98, an increase of 15 percent over JIMTOF '96. Nearly 90% of the spindles exhibited were lubricated using methods that keep lubricant consumption low. These methods included grease lubrication (37%), oil/air lubrication (37%), and oil mist lubrication (17%). Lubrication methods that require large amounts of lubricant and power, such as oil jet lubrication and under-race jet lubrication, were employed by only 5%, reflecting the trend toward environmental awareness. Also, signaling the increased popularity of high-speed bearings, 100 (60%) of the machines in JIMTOF '98 used hybrid ceramic angular contact ball bearings, up 10 percent over the preceding fair.

2.3 Spindle diameter and running speed

Figs. 3 (a) and (b) show the diameters and the maximum running speeds of the spindles of the machining centers exhibited in the 18th and 19th fairs whose $d_m n$ values were 600 000 or more. Accounting for 50% of the spindles, the spindle diameter distribution was concentrated between 65 mm and 70 mm (47 machines) and at 100 mm (32 machines). Maximum spindle speeds were

concentrated at 10 000 rpm (39 machines), 12 000 rpm (41 machines), 15 000 rpm (18 machines) and 20 000 rpm (19 machines), representing approximately 70% of the total number of machines. Compared to JIMTOF '96, nearly twice as many machines capable of both low-speed heavy-duty machining (rough cutting) and high-speed light-duty machining (finishing) were displayed at JIMTOF '98. Among the machines exhibited at JIMTOF '98, 16 machines used "Neobrid Bearings" (see Note 1) and nine machines used "Spinshot Bearings" (see section 4.2). Both of these bearings are variations of NSK hybrid angular contact ball bearings with improved high-speed performance. These machines have large-diameter spindles and are capable of high running speed and high $d_m n$ values.

Note 1: Neobrid Bearings are modified hybrid angular contact ball bearings with martensitic stainless steel inner rings. The lower linear expansion coefficient of the stainless steel gives these bearings improved temperature rise characteristics. For further details, see the NSK catalog, "Precision Neobrid Angular

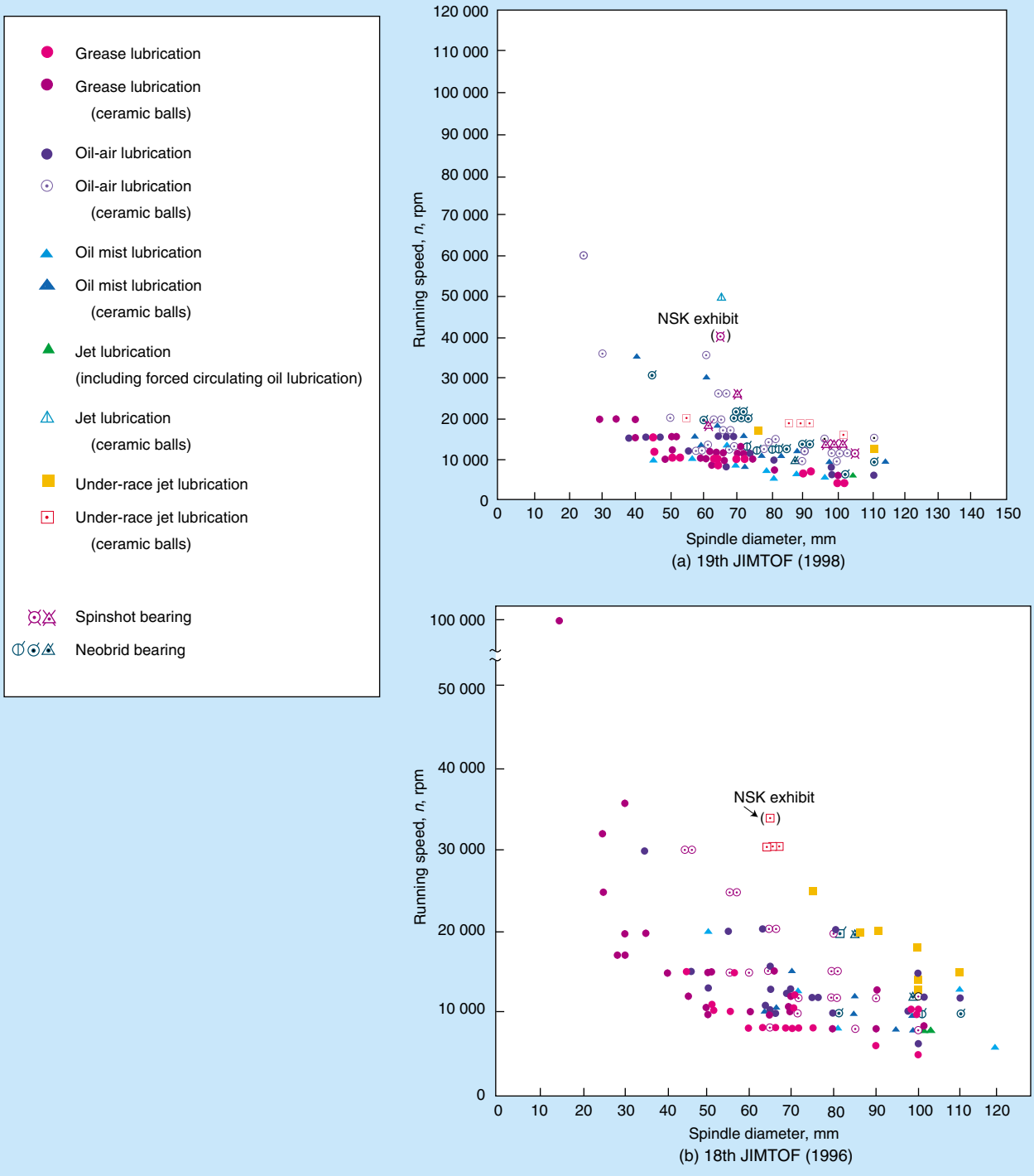

Fig. 3 Distribution of exhibited high-speed machining center spindles capable of 600 000 $d_m n$ or higher

Contact Ball Bearings for High-Speed Machine Tool Spindles" (Cat. No. E1204).

2.4 Summary of key trends at JIMTOF

(1) The number of machines with a $d_m n$ value of 600 000 or more and maximum running speed of 10 000 rpm or higher increased by 15% from the 18th JIMTOF to the 19th JIMTOF. The increase was particularly noticeable in machines with maximum speeds at useful levels of 12 000, 15 000 and 20 000 rpm. Looking only at rpm, spindle speed appears not to have increased much, but many of the exhibited machines had a spindle diameter one size larger to effectuate a substantial increase in rigidity. This requires spindle bearings to have higher $d_m n$.

(2) The number of machines employing oil jet or under-race lubrication for their spindle bearings was the same at the 19th fair as in the preceding fair. Reflecting the trend for environmental compatibility, the use of grease, oil-air and oil mist lubrication increased. Clearly, expectations are for spindle bearings to achieve higher speed and longer life with grease lubrication.

(3) Hybrid angular contact ball bearings were used in about 60% of the machines exhibited at the 19th fair (50% at the 18th fair). While hybrid bearings are becoming the standard for high-speed machines, their internal and surrounding structures and lubrication method need to be optimized.

As summarized above, trends in machine tools are for high rigidity with versatility, instead of merely high-speed performance. Demand is for machine tools capable of performing machining processes from low-speed heavy-duty rough cutting to high-speed light-duty finishing.

3. ROBUST Series Bearings with Improved Temperature Tolerance for Motorized Spindles

3.1 Necessity of temperature robustness

As mentioned in the foregoing section, machine tools today must be able to perform a series of operations, from rough machining to finishing, with high efficiency. To meet these requirements, it is essential for them to have high-speed performance and short start-stop time (i.e., high acceleration and deceleration) for fast and easy tool replacement. If a belt drive or a gear drive is used for a spindle with such capability, the power transmission will result in excessive heating, sliding and wear. If a direct driving motor and coupling are used, additional design requirements arise, such as the alignment between the motor and the spindle, the selection of a proper coupling and the method of holding the tools in place. Furthermore, the overall length of the spindle has to be longer, resulting in space restrictions and greater inertia. To avoid these disadvantages, recent machine tools have spindles with built-in motors (motorized spindles) that incorporate a compact and high-output rotor that minimizes inertia. However, motorized spindles are prone to greater exposure to changes in their surrounding environment (such as motor heating and sleeve cooling) particularly during sharp changes in rotating speed. These changes expose the bearings to severe thermal loads. It is understood that abrupt starts like cold starts of bearings produce a difference between the outer and inner ring temperatures (i.e., higher inner ring temperature than outer ring temperature). This temperature difference causes the reduction of the bearing clearances and, if the bearing is preloaded in a fixed position, tighter preload, which in turn raises heat generation and greatly increases the chance of bearing seizure. Consequently, bearings for motorized spindles are required to be robust enough to resist seizure and keep running stably while generating less heat under severe thermal load conditions. Essentially, the bearings must be insensitive to external thermal disturbances.

Meeting the severe requirements of motorized spindles, NSK's ROBUST Series angular contact ball bearings have excellent thermal robustness that is realized by their optimal internal design. The ROBUST Series is available in the four types whose material combinations and structures are shown in Fig. 4. The Series is also described in NSK catalog number E1221, "ROBUST Series High-Speed Precision Angular Contact Ball Bearings for Machine Tool Spindles."

Type	Inner ring material	Outer ring material	Ball material	Bearing construction
S Type	SUJ2	SUJ2	SUJ2	
H Type	SUJ2	SUJ2	Si_3N_4	
X Type	SHX	SHX	Si_3N_4	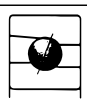
EX Type	SHX	SHX	Si_3N_4	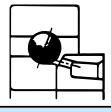

Fig. 4 Materials and construction of ROBUST Series

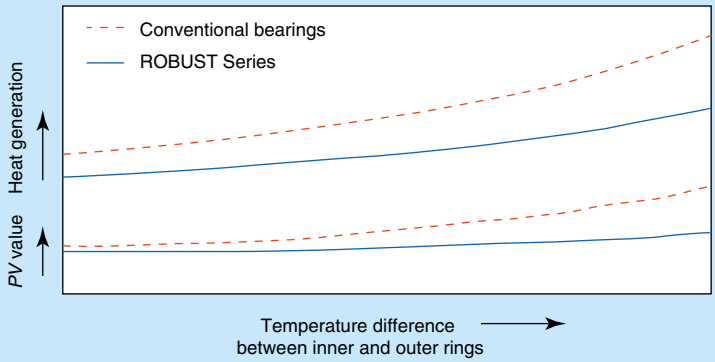

With less heat generation and a lower *PV* value, ROBUST Series bearings operate with greater stability than conventional precision bearings.

Fig. 5 Relation between inner and outer ring temperature difference and bearing heat generation and *PV* value

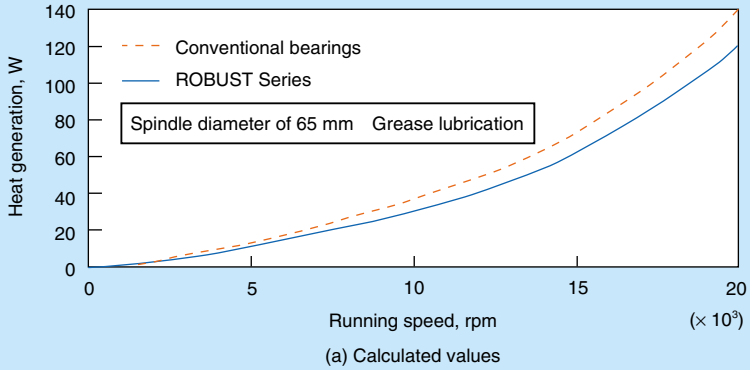

(a) Calculated values

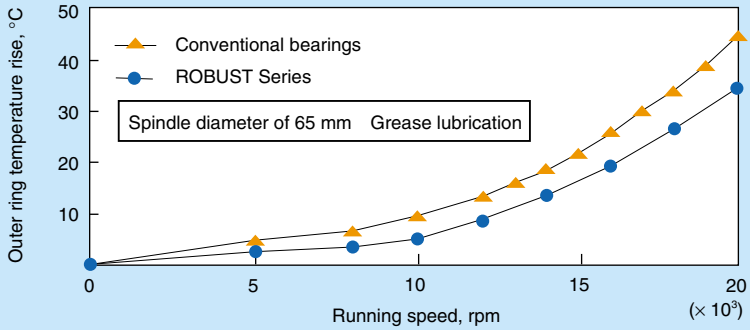

(b) Measured values

Fig. 6 Analysis and evaluation results on bearing dynamics

3.2 Improved thermal robustness and low heat generation

(1) Improved thermal robustness

Under machining conditions involving changes in rotational speed and cutting conditions, the internal temperature of machine tool spindles and consequently the bearings they contain significantly changes. These changes cause differences in outer and inner ring temperature that lead to reduced internal clearances. As internal clearances are reduced, the contact angles between the balls and the outer and inner ring raceways are changed sharply, the internal preload is increased and the *PV* value at rolling contact points between the outer and inner rings and balls is increased. The ROBUST Series was designed based on analysis of ball diameter, outer and inner ring groove curvatures, contact angles and other affecting factors to minimize bearing temperature change under such operating conditions.

(2) Low heat generation

Temperature differences that occur between the outer and the inner ring of a bearing during abrupt acceleration relate to the time-lag property of the heat transfer system around the bearing. Still, minimizing the heating of the bearing itself contributes to the improvement of the thermal displacement property, which is important for machine tools.

ROBUST Series bearings are designed to have minimum heat generation in addition to the improved robustness described above. This low heat-generating property is further enhanced through the use of a unique bearing material called SHX,[2] a carburized nitrided steel developed by NSK.

3.3 Test results

Fig. 5 compares calculated heat generation and *PV* values of ROBUST and conventional bearings as a result of changes in temperature difference between their outer and inner rings. Illustrating the stable operating performance of the ROBUST Series, the increase of these values is much smaller than for the conventional bearings. Fig. 6 (a) compares calculated results and Fig. 6 (b) compares measured results on power loss of the two types of bearings. Calculated results showed good agreement with measured results.

Fig. 7 compares the temperature rise under grease lubrication of conventional hybrid angular contact bearings and the newly designed ROBUST H type. The temperature rise of the newly designed bearing is 20% lower than that of the conventional bearings when operated at the same speed. In fact, to reach the same level of temperature rise, the H type must be operated at 20% higher running speed than the conventional bearing. Additionally, when tested without sleeve cooling, the temperature rise of the outer ring was only 15°C at a running speed of 15 000 rpm ($d_m n$ = 1 200 000) and at a running speed of 23 000 rpm ($d_m n$ = 1 900 000), no seizure occurred and the temperature was stable.

Fig. 8 compares the temperature rise during operation with oil-air lubrication. When the sleeve is cooled, the maximum running speed is lower than when it is not cooled because of a greater increase in the difference between the outer and inner ring temperatures. Still, the newly designed bearing achieved a maximum speed of 18 000 rpm ($d_m n$ = 2 000 000) with sleeve cooling. Further demonstrating the viability of the new bearing, the outer ring temperature rise was only about 15°C, in spite of a preload of 392 N (40 kgf) at assembly, which is relatively high for high-speed spindles.

4. Improved Seizure Resistance with New SHX Material

Environmental requirements for machine tool spindles include the reduction of power consumption by reducing spindle power loss and the minimization of the use of lubricants and other materials that can harm the environment. In meeting these requirements, first consideration should be given to reducing the use of

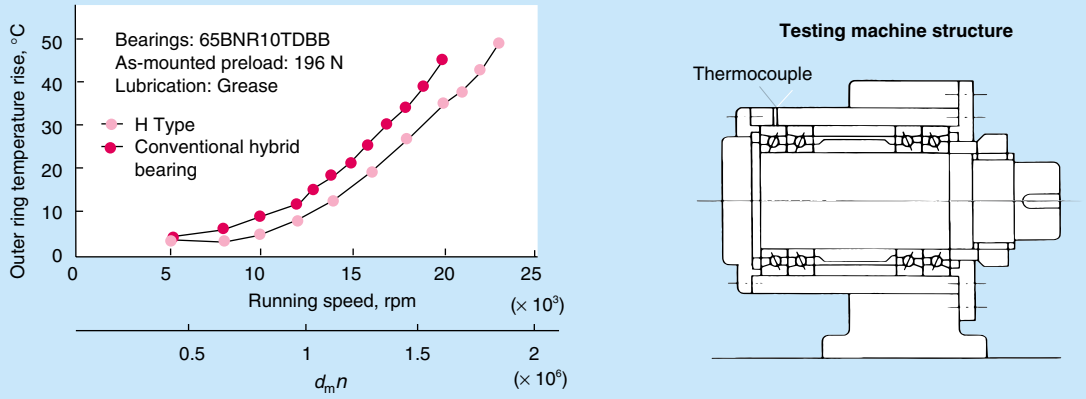

Fig. 7 Comparison of temperature rise with grease lubrication (H Type and conventional)

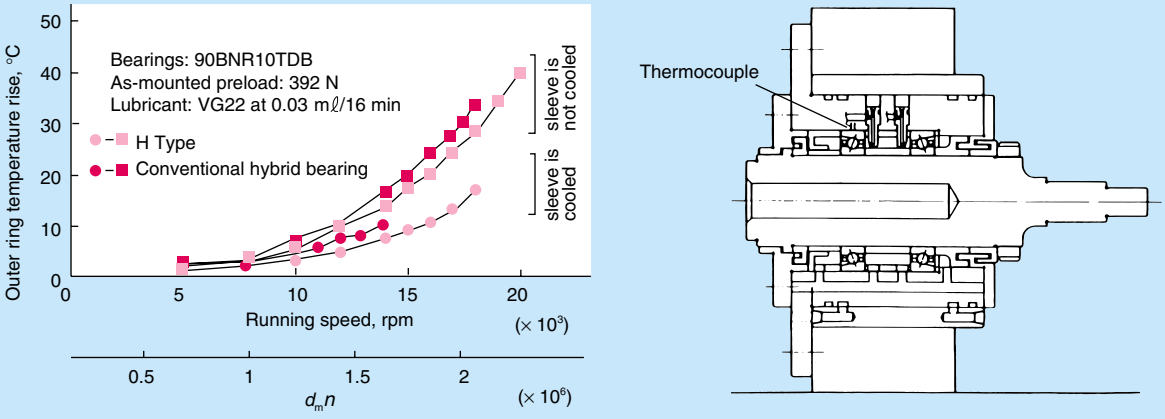

Fig. 8 Comparison of temperature rise with oil-air lubrication (H Type and conventional)

lubricants. It is understandable, therefore, that more of the machines exhibited at JIMTOF '98 than past fairs employed grease, oil-air or oil mist lubrication—all methods that use relatively small amounts of lubricant—instead of oil jet or under-race lubrication, which both consume large amounts of lubricant. However, these lubrication methods that use small amounts of lubricant do not ensure adequate cooling and may give rise to temporary and/or local lubricant shortage on rolling contact surfaces. When local lubricant starvation occurs, metal-to-metal contact leads to heat generation and deterioration of the material's physical properties (e.g., reduced hardness). As a result, the frictional coefficient increases and further heating occurs. This may eventually lead to bearing seizure.

Even under the lubricant-starved conditions described above, NSK's unique new SHX material exhibits excellent seizure and wear resistance and long life. The following sections outline test results on bearings with SHX inner and outer rings. For the properties of SHX, refer to the article in Reference 1.

4.1 Test results on bearings with SHX outer and inner rings

Fig. 9 presents temperature rise data under grease lubrication on new ROBUST Series X type hybrid angular contact ball bearings, whose outer and inner rings are made with SHX steel. The temperature rise of these bearings was lower than the conventional bearings and the temperature of the SHX bearings was more stable, even when operated at 25 000 rpm (2 000 000 in $d_m n$ value).

4.2 Spinshot™ lubrication system

EX-type ROBUST Series bearings feature NSK's exclusive Spinshot™ lubrication system, a unique under-race lubrication system with a special inner ring spacer (Fig. 10). Oil-air (a mixture of a small amount of oil and compressed air) is fed from the lubrication device to the bearing via nozzles and oil scoops in the spacer. The nozzles in the spacer are inclined outward so that centrifugal force makes the oil flow into the bearing with greater velocity as speed increases. With the Spinshot™ spacer, the steady supply of lubricant and the cooling effect of the oil-air mixture greatly increase the limiting speed of the bearing. With SHX material and the Spinshot™ lubrication system, ROBUST Series EX bearings have excellent seizure resistance and high-speed performance. Fig. 11 shows test results on EX bearings operating under position preload. For bearings preloaded in a fixed position, 2 000 000 $d_m n$ was formerly only attainable with oil jet lubrication or under-race jet lubrication. With the Spinshot™ lubrication system, 2 400 000 $d_m n$ (27 000 rpm) was achieved. Fig. 12 shows test results on the same bearings under constant preload.

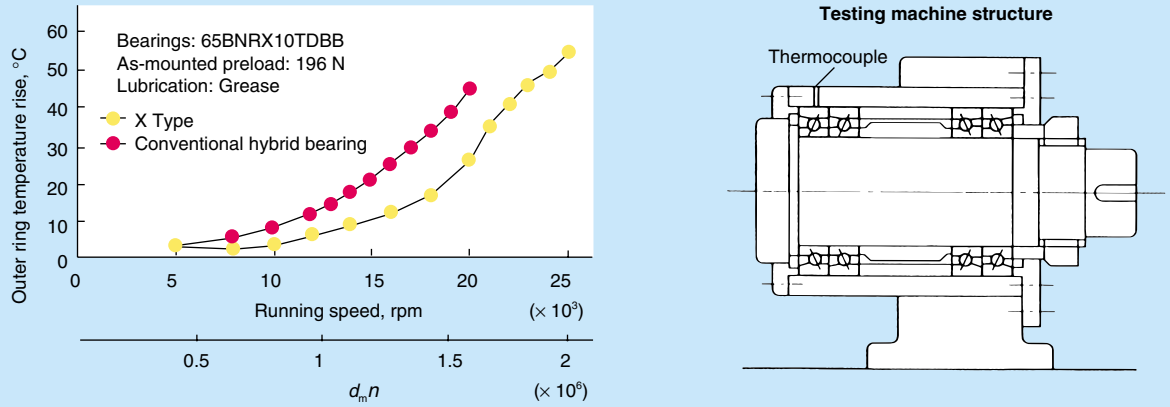

Fig. 9 Comparison of temperature rise with grease lubrication (X type and conventional)

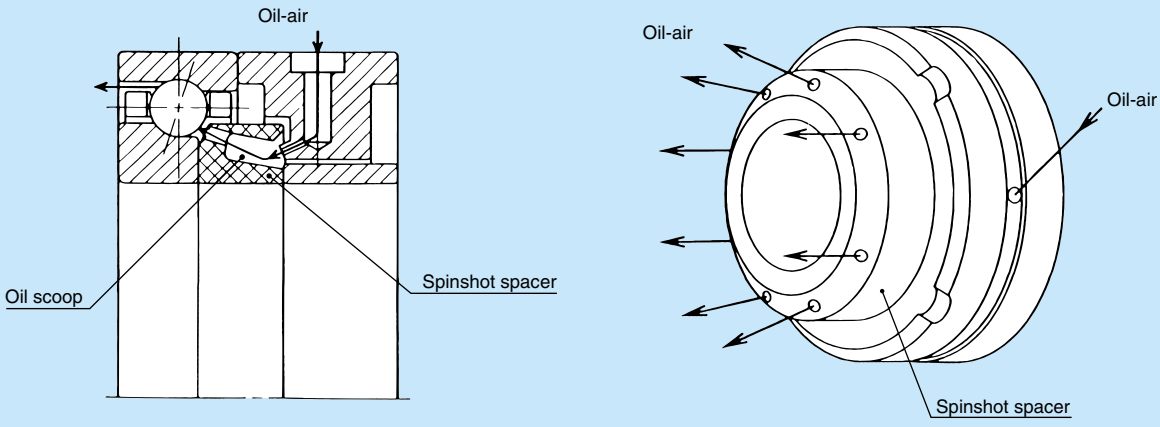

Fig. 10 Spinshot™ lubrication system

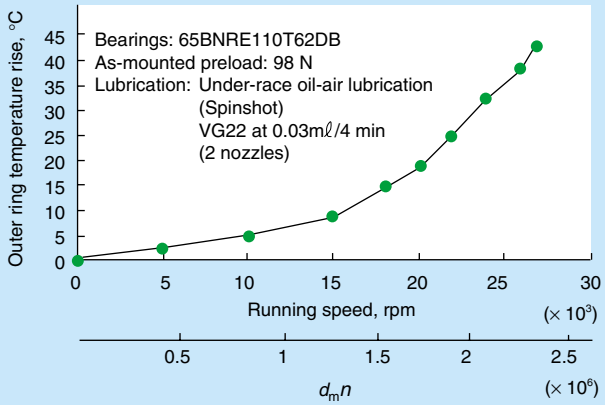

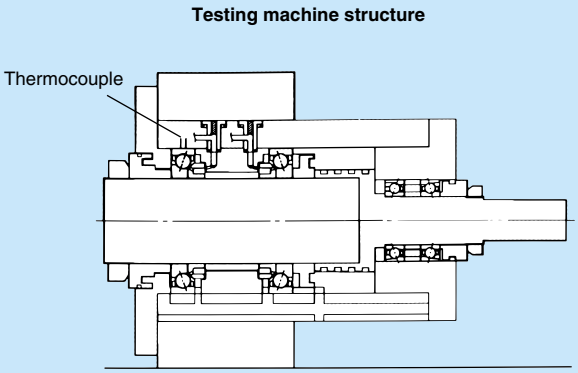

Fig. 11 Temperature rise of EX Type with oil-air lubrication under position preload

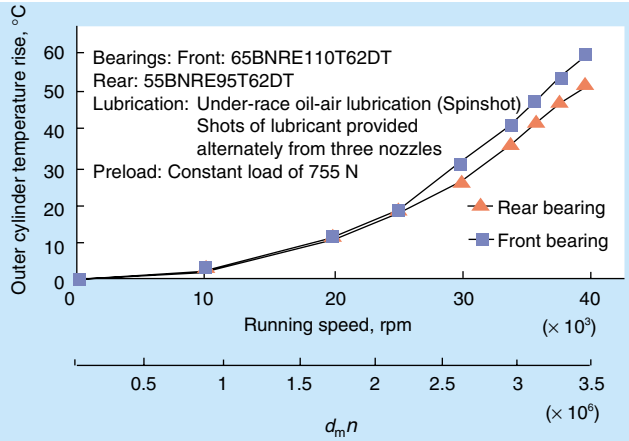

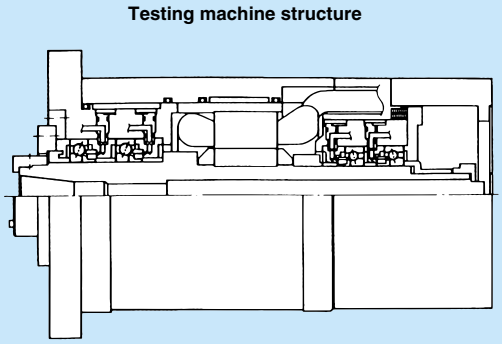

Fig. 12 Temperature rise of EX Type with oil-air lubrication under constant-load preload

The test machine was an actual motorized spindle, identical to one exhibited at JIMTOF '98. The extremely high speed of 40 000 rpm (3 500 000 $d_m n$) was realized in the test.

5. Conclusion

As demonstrated every other year at JIMTOF, the trend of machine tools toward higher-speed operation with greater efficiency is clear. NSK's ROBUST Series responds to this trend by offering a range of solutions for the machine tools of the 21st century.

References:

1) Y. Ohura, M. Kameko, A. Dodd, N. Mitamura and H. Kawamura, Development of Jet-Engine Bearings (Part 2), NSK Technical Journal, 667 (1999), 7–13. [in Japanese]
2) H. Yoneyama: Rolling Bearing Themes for High-Speed Spindles, Proceeding of the Seminar, New Technology for High-Speed Machine Tools, 1998.11.27., the Japan Society of Mechanical Engineers [in Japanese]

Yukio Ohura

Yoshiaki Katsuno

Sumio Sugita

Development of the POWERTOROS UNIT Half Toroidal CVT

Hisashi Machida and Yasuo Murakami
Research and Development Center

1. Introduction

NSK started development of its traction drive half toroidal CVT (Continuously Variable Transmission) in 1978 and succeeded in commercializing it in Nissan Motors' Cedric and Gloria models in November 1999. In this report, we discuss the history of research and development work over the past 21 years, the technical features of the traction drive half toroidal CVT and the product's future prospects.

2. History of the Toroidal CVT

Charles W. Hunt of Richmond, New York, U.S.A., was the first in the world to conceive of the principle of the toroidal CVT. His invention is contained in U.S. patent 197 472, November 27, 1877. In the patent (Fig. 1), an oscillating wheel (E) is placed between disks B and D. By varying the angle of this wheel, speed is changed. The surfaces of disks B and D are spherical. As this structure is very simple, industrial use was attempted. With the appearance of automobiles, application in automotive transmissions was examined and in the 1920s many samples were made and sold. A car called a "friction drive car," which was equipped with such a mechanism, was even produced, though it did not meet much commercial success. Then, in 1943, Wright Aeronautical devised the half toroidal CVT. Wright acquired a patent from Charles E. Kraus in 1959 and developed the CVT shown in Fig. 2. They conducted many bench tests and tests in actual cars. Kraus pointed out that reducing the spin at the contact point that transmits power not only increases the size of the contact point surface but also contributes to improved transmission efficiency and endurance and reduced size. In 1973, at Traycall, Texas, Charles Kraus and his son James conducted tests on a traction drive CVT installed in a Ford Pinto with 85 HP.[1)] At that time the transmission ratio of the CVT was from 2.65:1 to 0.6:1 (transmission ratio range 4.417). From the results of this test, they anticipated that the CVT was capable of realizing good acceleration, high fuel efficiency and cleaner vehicle emissions. In 1978, applying lessons learned from the Oil Shock and considering Professor Tomoo Ishihara's (Institute of Industrial Science, University of Tokyo) suggestion that automatic transmission would shift to the CVT because of its higher fuel efficiency, NSK Ltd. started research and development on the half toroidal CVT jointly with Professor Ishihara's research group.

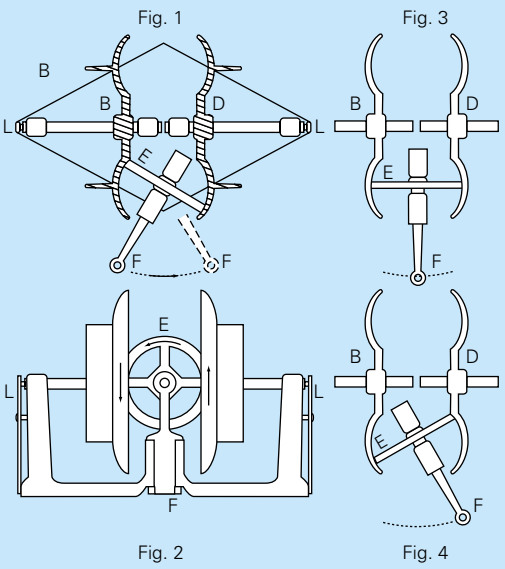

Fig. 1 The first patent on the toroidal CVT

3. Basic Structure of the Toroidal CVT

3.1 Geometrical particularities

The toroidal CVT is classified into two types by its shape: full toroidal CVT and half toroidal CVT. Fig. 3 shows an example of the full toroidal CVT. The particularities of the geometry of this type lie in the fact that the straight line OO' that passes between the contact points of the power roller with the input and output disks passes through the center of the cavity circle forming the input and output disks. As a result, the reaction force to the contact force generated for power transmission between the power roller and input/output disks does not apply to the sustaining bearing of the power roller. On the other hand, as each of the lines tangent to the contact points O, O' is parallel and has no point of intersection, the spin of the contact point becomes large. Fig. 4 shows the schematic geometry of the contacting part of the half toroidal CVT. In this type, each of the lines tangent to the contact points O, O' has the point of intersection E and when this point E is on the rotation axis I, the spin of contact points O, O' becomes 0. The spin loss of the half toroidal CVT is smaller than the full toroidal CVT shown in Fig. 3 because the locus of the point of intersection E is nearby the rotation axis I for the entire range of the transmission and zero spin can be realized with the half

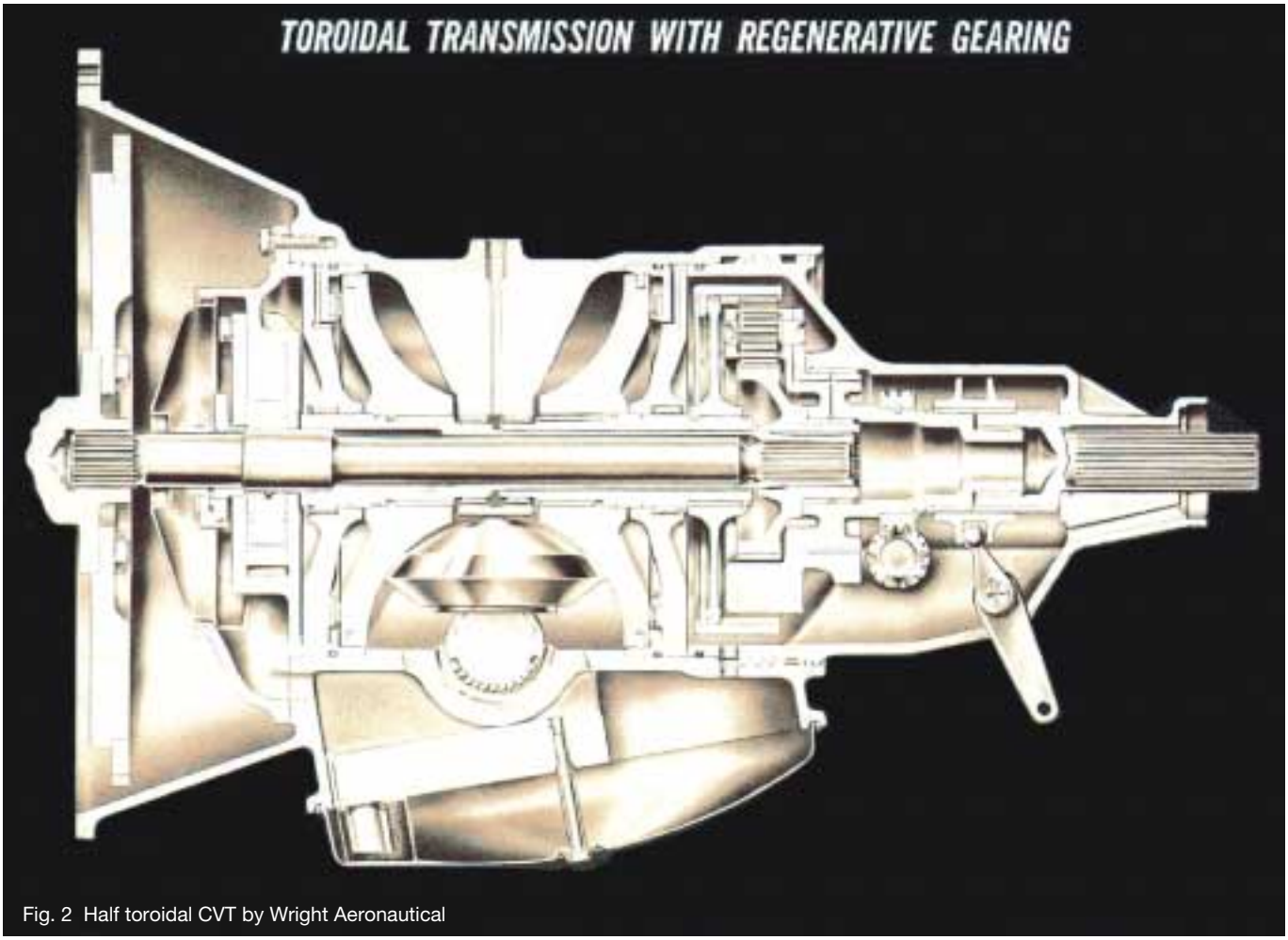

Fig. 2 Half toroidal CVT by Wright Aeronautical

toroidal CVT. Using the symbols in Fig. 4, the spin ω_{SP} at point O can be given by this Equation (1):

$$\omega_{SP} = \omega_1 \sin \phi_0 - \omega_2 \cos\theta \quad \ldots\ldots\ldots\ldots\ldots\ldots (1)$$

where

ω_1: Speed of input disk (rad/s)
ω_2: Speed of power roller (rad/s)
ϕ_0: Inclination angle (rad)
θ: Power roller opening half cone angle (rad)

Fig. 5 shows a cross-section of the half toroidal CVT. This type is a single cavity with only one cavity circle and the disk sustaining bearing **9** must accommodate the axial force acting on the disk. In addition, as the straight line OO' of Fig. 4 does not pass the center point of the cavity circle, the power rollor bearing **8** must sustain the axial force of the power roller and forces in the axial direction of the input/output disks.

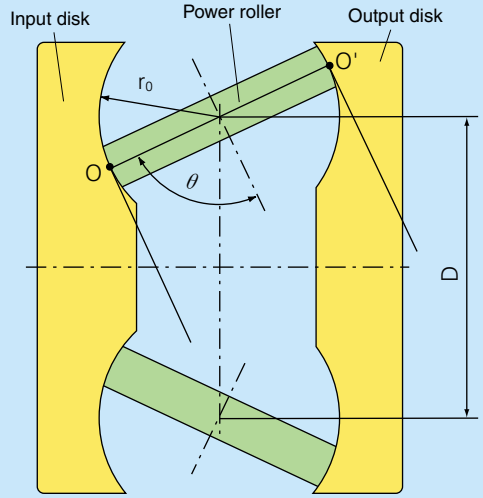

Fig. 3 Full toroidal CVT

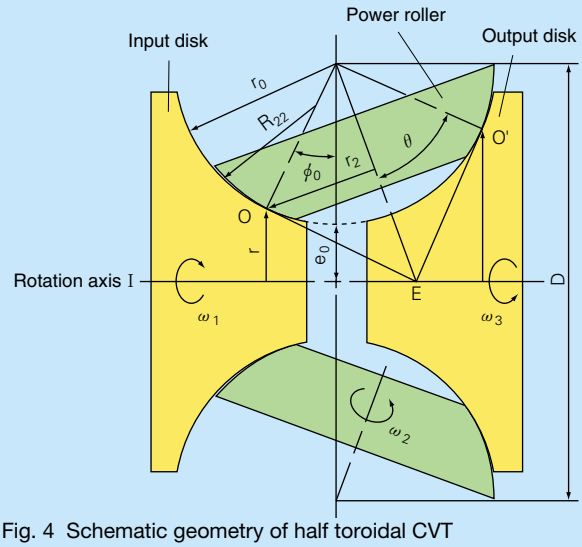

Fig. 4 Schematic geometry of half toroidal CVT

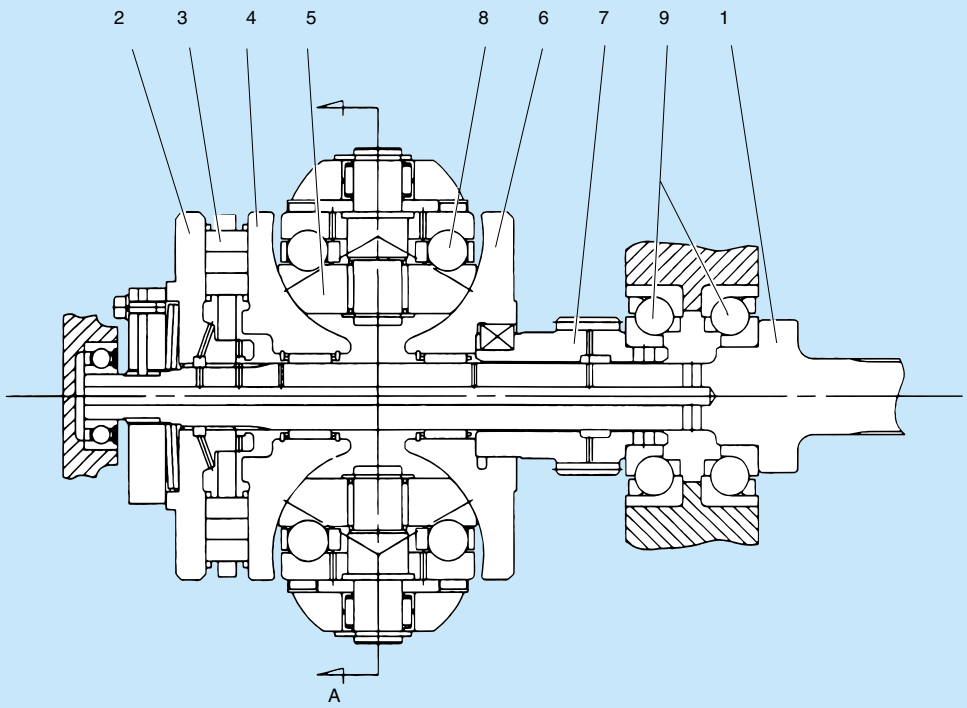

Fig. 5 Half toroidal CVT

3.2 Transmission ratio

From Fig. 4 each radius of rotation is given as follows

$$R_1 = R_{12}\,(1 + k - \cos\phi_0) \quad \ldots\ldots (2)$$
$$R_2 = R_{12} \sin\theta \quad \ldots\ldots (3)$$
$$R_3 = R_{12}\,\{(1 + k - \cos(2\theta - \phi_0)\} \quad \ldots\ldots (4)$$
$$k = D_{cav} / (2R_{12}) - 1 \quad \ldots\ldots (5)$$

where

R_1: Radius of rotation to contact point of input disk (m)
R_2: Radius of rotation to contact point of power roller (m)
R_3: Radius of rotation to contact point of output disk (m)
R_{12}: Radius of major curvature of input/output disks (m)
D_{cav}: Diameter of toroidal cavity (m)

and the transmission ratio i is given by Equation (6):

$$i = R_3/R_1 = \{1 + k - \cos(2\theta - \phi_0)\} / (1 + k - \cos\phi_0) \quad \ldots\ldots (6)$$

3.3 Power transmission

Next, using Fig. 5, we illustrate the power transmission system. The power input to the input shaft is transmitted in order to the loading cam, cam roller, input disk, power roller, output disk and output gear. The contact point of the input disk with the power roller, i.e., point O in Fig. 4, is in fact elliptical based on the theory of Hertz and its semi-major axis a and semi-minor axis b are given by:

$$a = n \sqrt[3]{3Fc/(E'\,\Sigma\rho)} \quad \ldots\ldots (7)$$
$$b = m \sqrt[3]{3Fc/(E'\,\Sigma\rho)} \quad \ldots\ldots (8)$$
$$E' = 2 / \{(1 - \nu_1^2)/E_1 + (1 - \nu_2^2)/E_2\} \quad \ldots\ldots (9)$$
$$\Sigma\rho = 1/R_{11} + 1/R_{12} + 1/R_{21} + 1/R_{22} \quad \ldots\ldots (10)$$

where

F_c: Contact force (N)
E_1: Young's modulus of input disk (N/m^2)
E_2: Young's modulus of power roller (N/m^2)
ν_1: Poisson's ratio of input disk
ν_2: Poisson's ratio of power roller
R_{11}: Radius of principal curvature of input disk (perpendicular direction to the space in Fig. 4, m)
R_{12}: Radius of principal curvature of input disk (parallel direction to the space in Fig. 4, m)
R_{21}: Radius of principal curvature of input disk (perpendicular direction to the space in Fig. 4, m)
R_{22}: Radius of principal curvature of power roller (parallel direction to the space in Fig. 4, m)
n, m: Coefficients obtained by elliptic integral

The mean surface pressure at the contact point is given by Equation (11):

$$P_{mean} = F_c / (\pi ab) \quad \ldots\ldots (11)$$

The transmission torque and traction force at point O are given by the following:

$$T_0 = R_1 F_t \quad \ldots\ldots (12)$$
$$F_t = \mu F_c \quad \ldots\ldots (13)$$

where

T_0: Transmission torque (N・m)
F_t: Traction force (N)
μ: Traction coefficient

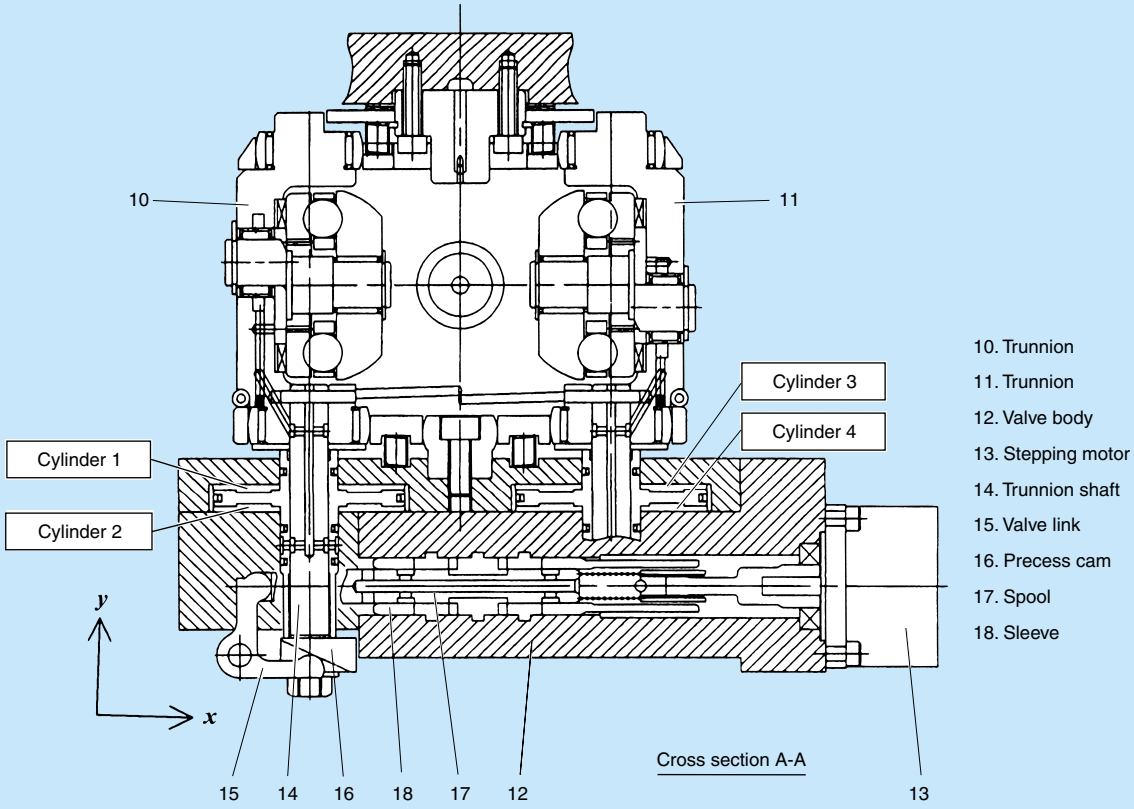

Fig. 6 Half toroidal CVT

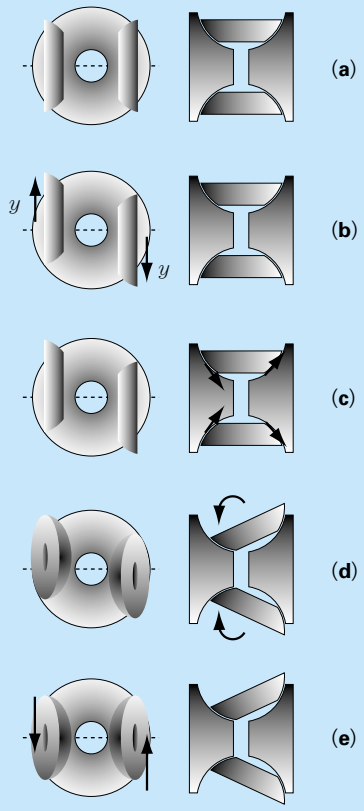

Fig. 7 Control principle of transmission of half toroidal CVT

The contact force, F_c, is obtained as a component of the axial force, F_a, of the loading cam. F_a is generated proportionally to the input shaft torque:

$$F_c = F_a / (n / \sin \phi_0) \quad \ldots\ldots (14)$$

$$F_a = 2\pi \cdot T_0 / L_c \quad \ldots\ldots (15)$$

where

n: Power roller number

L_c: Loading cam lead (m)

3.4 Balance of forces

Fig. 6 shows the A-A cross-section of Fig. 5. The reaction force to the traction force acting on the trunnions is received by the hydraulic force of four hydraulic cylinders. When power is transmitted between the disks and power rollers and all rotation axis lines of the power rollers intersect with the rotation axis lines of the disks, the balance of y-axis direction is given by Equation (16):

$$2F_t = P_H \cdot A - P_L \cdot A \quad \ldots\ldots (16)$$

where

P_H: Hydraulic force of cylinders 1, 4 (Pa)

P_L: Hydraulic force of cylinders 2, 3 (Pa)

A: Area of surface of cylinder receiving pressure (m^2)

Hydraulic force is fed from the external pump. Cylinders 1 and 4, and 2 and 3 are connected by respective piping. This pressure is controlled by the transmission control valve.

3.5 Transmission control mechanism

Transmission control of the half toroidal CVT is performed by control of the inclination angle of the power roller, as shown in section 3.2. To incline the power roller, a motion vector in the inclined direction at the rolling contact part is generated by displacing the power roller's central axis in the y-axis direction (Fig. 6). The inclination force is obtained by the sideslip generated on this contact point at that time. Fig. 7-(a) shows the state of the power transmission when acting forces are balanced as the roller rotation axis line and the disk rotation axis line intersect. When the sleeve of the control valve is displaced in the x-axis direction by means of the stepping motor, pressures P_H and P_L change and the trunnions move in the y-axis direction (in the opposite direction) (Fig. 7-(b)), and the contact points of the disks and power rollers change. By this process, slant rotation force is generated (Fig. 7-(c)) and the right and left trunnions slant in a symmetrical direction (Fig. 7-(d)). A sensor rod is mounted on one of the trunnions and the precess cam is mounted on the top of the rod. The precess cam converts the slant amount to the motion of the spool of the control valve in the x-axis direction (same direction as the sleeve) through the link. The precess cam moves the spool to correct the displacement of the sleeve and to change the pressure and when the force of Equation (16) is balanced, slanting is stopped (Fig. 7-(e)). Therefore, the force necessary to shift the transmission is only that to activate the sleeve of the control valve. A key feature of this hydraulic servo system is that the controlling force is not affected at all by the magnitude of the transmitted force. For running experiments in actual cars, we used a small stepping motor.

3.6 Loading cam

As means to generate contact force, there are a hydraulic system and a mechanical system. With the hydraulic system, precise control of the contact force depending on the torque is easy, but when installing this system in a car, due to space restrictions, the pressure-receiving surface is limited and high hydraulic pressure becomes necessary. As a result, the cost of the pump and its power loss become problems. To apply the half toroidal CVT to cars, we adopted a mechanical mechanism using a combination of a pressure-regulating conical disk spring and loading cam. At the contact points O and O' in Fig. 4, force is transmitted by traction drive. Now let's think about point O, for which the generated traction force is given as follows:

$$F_t = \mu \cdot F_c \quad \ldots\ldots\ldots\ldots\ldots\ldots\ldots\ldots (17)$$

and transmitted torque is as follows:

$$T_0 = n \cdot R_1 \cdot F_t \quad \ldots\ldots\ldots\ldots\ldots\ldots\ldots (18)$$

From Equations (17) and (18), the necessary contact force to transmit the input shaft torque is given as follows:

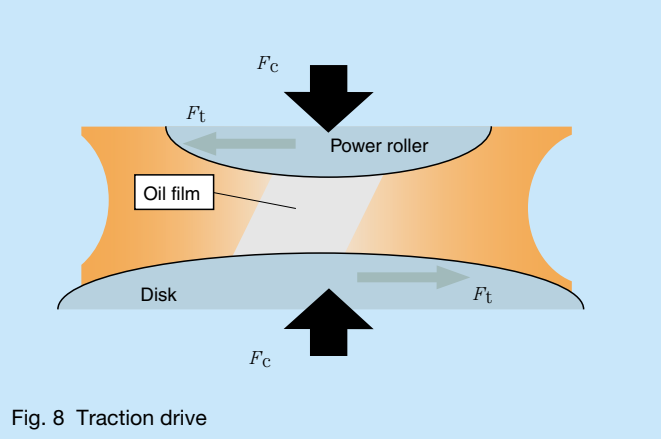

Fig. 8 Traction drive

$$F_{CN} = T_0 / (n \cdot R_1 \cdot \mu) \ldots\ldots\ldots\ldots\ldots\ldots (19)$$

by substituting this for Equation (2), the contact force required at all the gearbox ratios is expressed as follows:

$$F_{CN} = T_0 / \{(n \cdot \mu \cdot R_{12} (1 + k - \cos \phi_0)\} \ldots\ldots (20)$$

To generate contact force at the contacting part, two kinds of axial force-generating mechanisms are provided with the pressure-regulating conical disk spring and loading cam. The pressure-regulating conical disk spring is to secure the minimum contact force to satisfy the traction drive function at the contact point even when the input shaft torque is zero or very small. The loading cam starts to work when the input shaft torque exceeds a certain fixed value that is higher than the function range of the pressure-regulating conical disk spring. The loading cam and input shaft are connected by a spline. The loading cam is twisted by the input shaft and generates axial force as the cam roller rolls over the cam face. With this force the input disk is pushed forward and pushed up against the power roller. The contact force at the contact point is obtained in this way.

4. Traction Drive

Force transmission by means of traction drive is performed by the shearing force of an elastohydrodynamic lubrication oil film standing between two rotating bodies, as shown in Fig. 8. The thickness of the fluid film can be calculated based on the theory of Hamrock-Dowson,[2] and central oil film thickness h_c is about 0.4 (μm) under the conditions of contact surface pressure P_{max} = 2.2 (GPa), surface speed U = 24.2 (m/sec) and oil temperature 120°C. The relation between contact force, F_c, and tangential force, T_t, is as shown in Equation (13). The viscosity of the traction fluid between two rotating bodies increases suddenly under high contact surface pressure, becoming solid to transmit the force.

On the mechanism of traction generation, as the EHL theory was developed, various theoretical clarifications were attempted. In 1977 a rational explanation was given

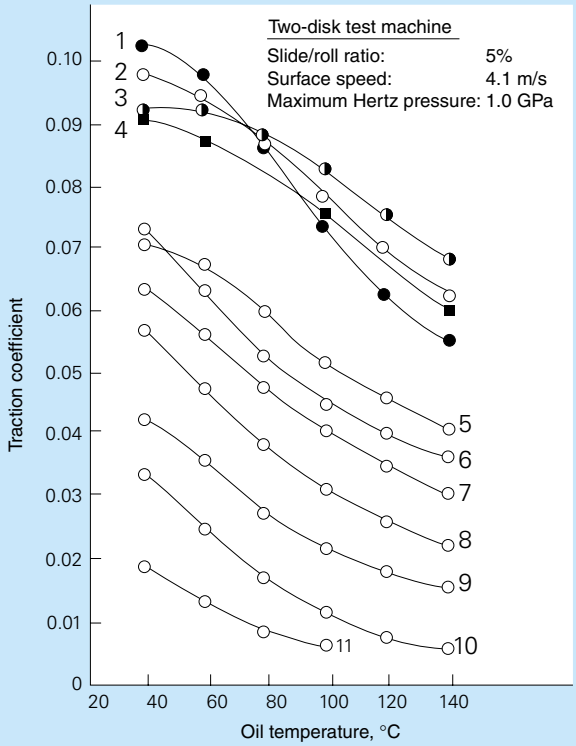

1. Commercialized synthetic traction oil
2. Idemitsu's synthetic traction oil
3. Idemitsu's synthetic traction oil
4. Idemitsu's synthetic traction oil
5. Alkylbenzene (hard)
6. Commercialized synthetic traction oil
7. Naphthenic mineral oil
8. Naphthenic mineral oil
9. Paraffinic mineral oil
10. Commercialized synthetic engine oil
11. Poly α olefin

Fig. 9 Traction coefficient of various oils

by Johnson et al.[3] They formulated the mechanism of traction generation using the elastic-plastic model of oil and they classified the motion in the EHL contact interface into three kinds, namely, slip, sideslip and spin.[4] In subsequent studies,[5] traction fluid under high pressure was considered as the non-linear Maxwell rheology model based on the Eyring theory, the existence of limiting shearing force was empirically confirmed and the traction fluid constitutional diagram was drawn, and the mechanism of traction drive was rapidly clarified. Tanaka used those theories and theoretically analyzed transmission efficiency in the traction drive power transmission unit.[7]

5. Traction Oil

The special synthetic traction oil indispensable to traction drive was developed by Monsanto of the U.S.A. in 1978. This was cycloalkylbenzene-based synthetic oil. Its maximum traction coefficient is 0.095, higher than naphthenic oil. In 1987, Hata and Aoyama of Idemitsu

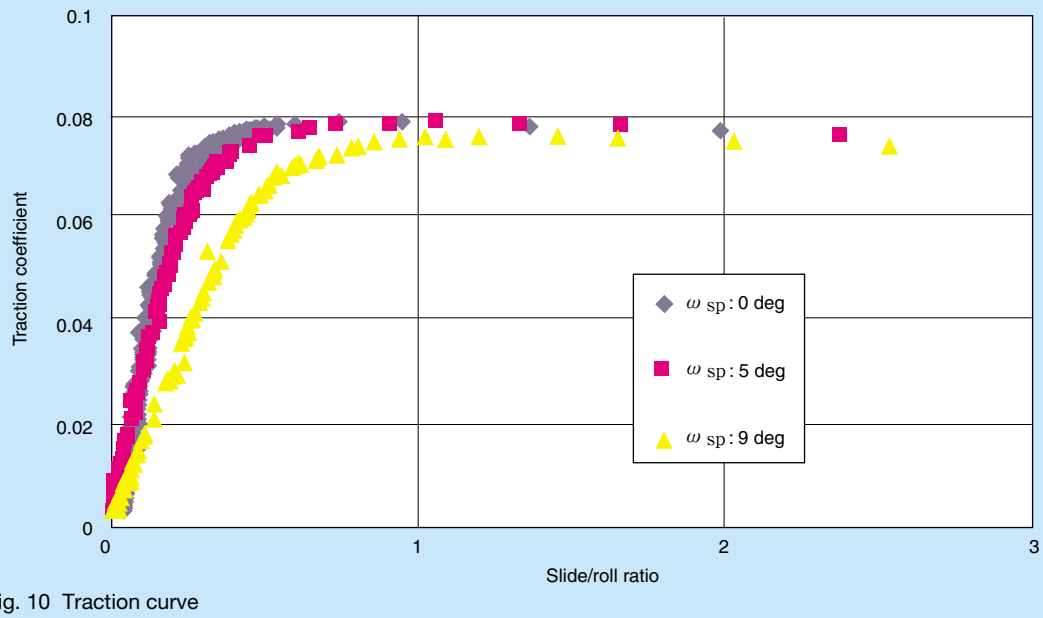

Fig. 10 Traction curve

Fig. 11 Requirements of traction oil

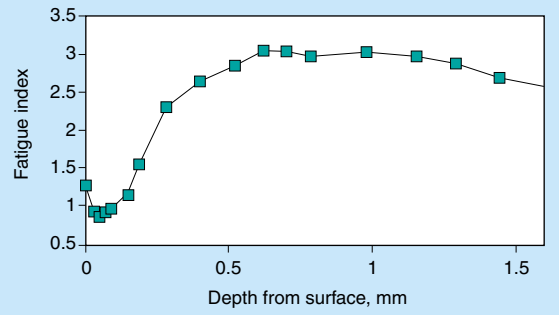

Fig. 12 Fatigue index of the disk

Kosan measured the traction coefficient of various oils under 40°C to 140°C, supposing application in traction driven automobiles. They used a two-cylinder test machine that produced 5% constant sliding (creep) (Fig. 9). Their results showed that oil with low temperature dependency and a high traction coefficient under high temperature was suited for use in automobiles. Then, NSK Ltd., (Natsumeda and Achiha) developed a two-cylinder test machine that could measure an oil's traction coefficient under conditions replicating actual cars.[8] Fig. 10 shows an example of the evaluation test. Traction characteristics were measured when spin was varied in the contact interface. Because only one kind of oil is used in the CVT, the oil must not only have a high traction

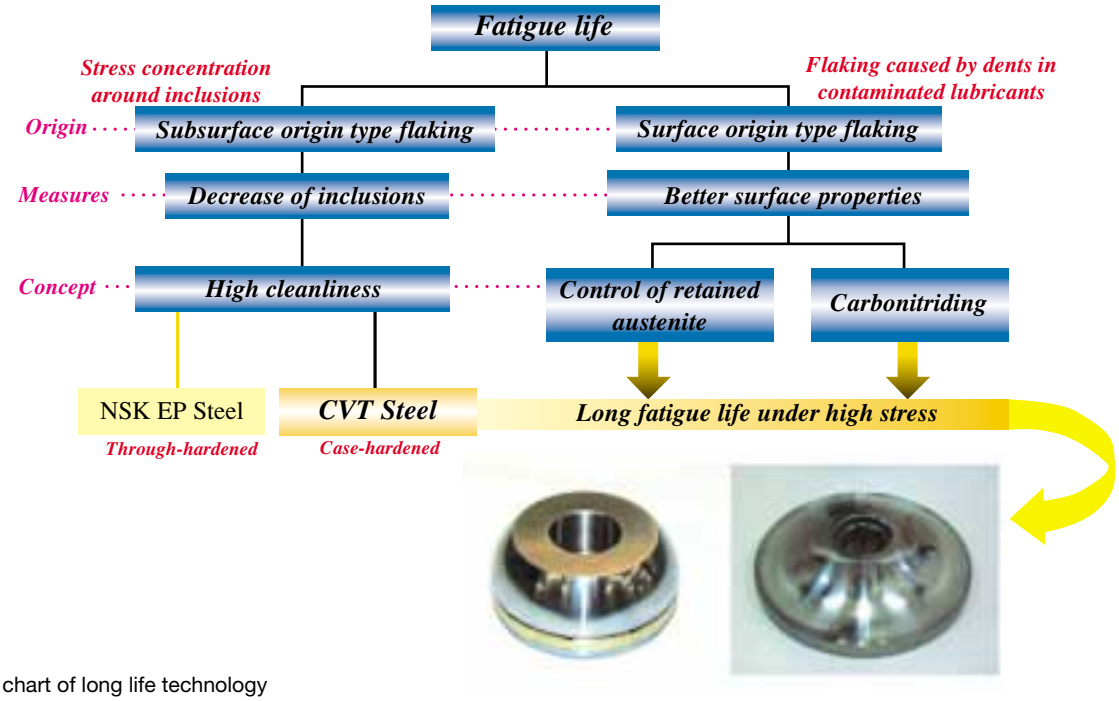

Fig. 13 Flow chart of long life technology

coefficient but also the diverse characteristics listed in Fig. 11. Development of traction oil for the CVT was a great technical challenge.

6. Endurance Reliability

Fig. 12 shows fatigue analysis results on the disk after completion of the endurance test. When fatigue is evaluated using the fatigue index,[9] it becomes clear that the fatigue of traction drive CVT components is very severe both externally and internally. Thus, we had to determine measures to prolong rolling contact fatigue life of traction drive CVT components operating under high surface pressure and to improve resistance to both surface- and subsurface-originating flaking.

Fig. 13 shows the technology for long-life bearings. For subsurface-originating flaking, we applied technology from

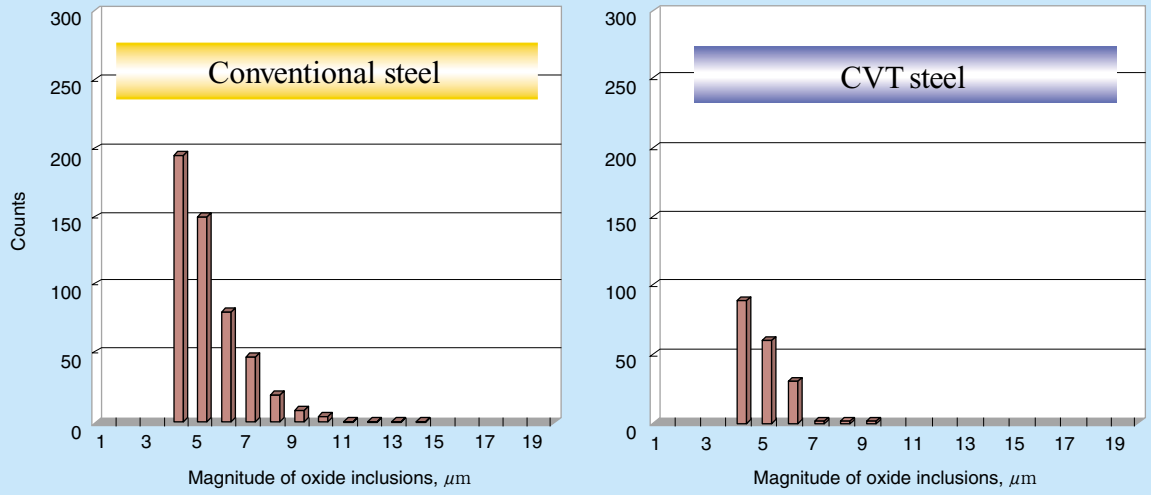

Fig. 14 Extra purified steel

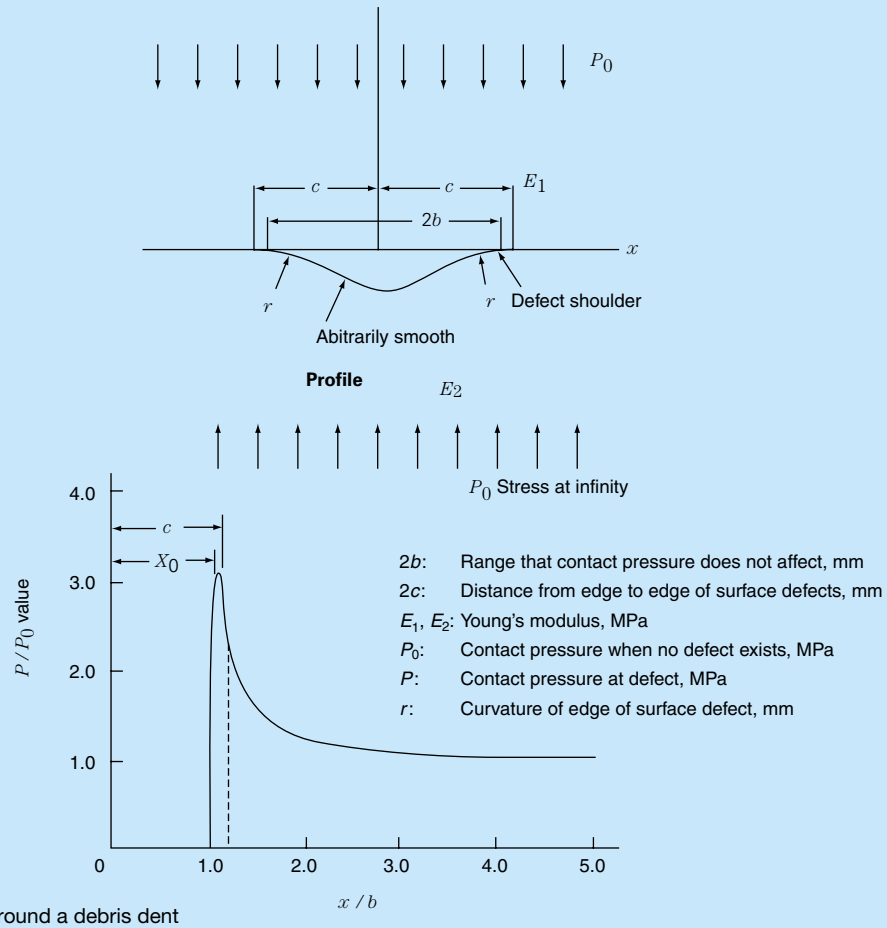

Fig. 15 Stress concentration around a debris dent

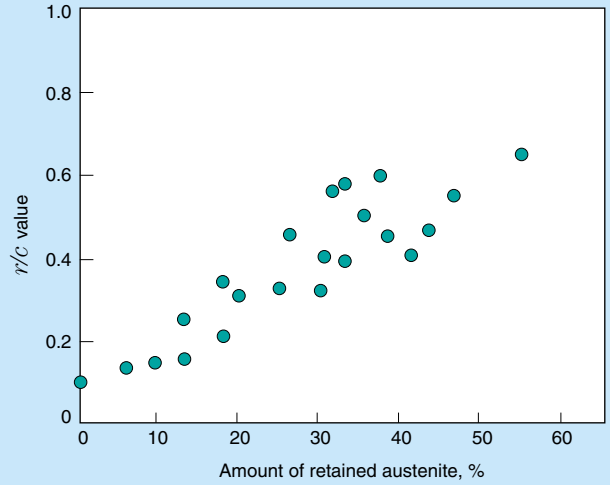

Fig. 16 r/c value vs. amount of retained austenite

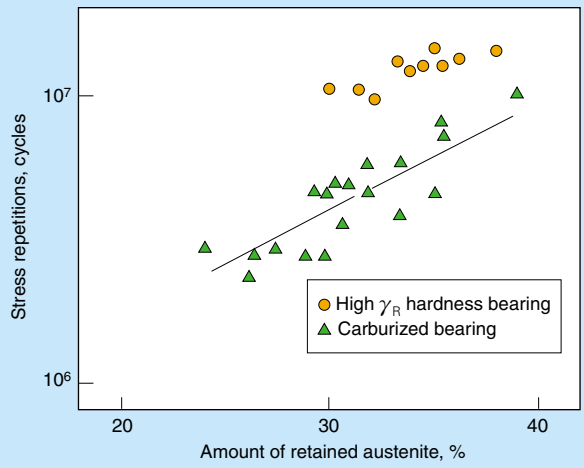

Fig. 17 Life vs. amount of retained austenite

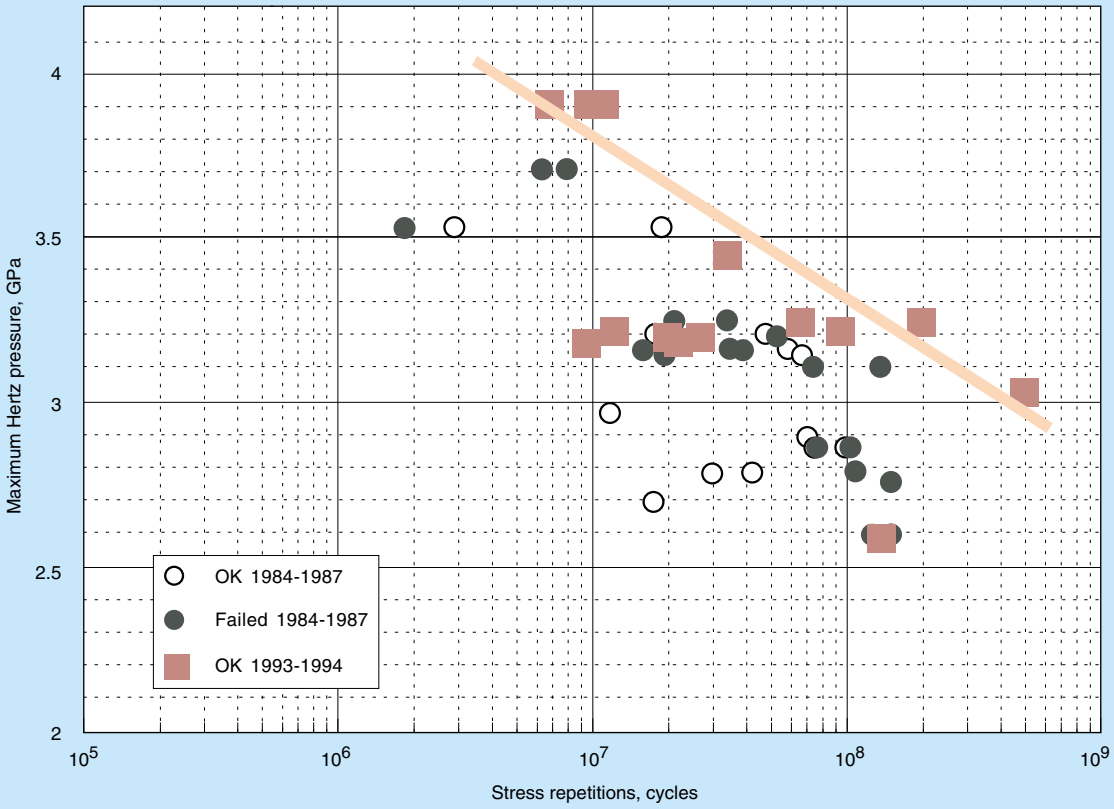

Fig. 18 Extra purified steel

SUJ2EP steel and reduced the non-metallic inclusions that become origin points of flaking. Next, we developed CVT steel for which the amount, magnitude and distribution of non-metallic inclusions are controlled. Fig. 14 shows the distribution of oxide inclusions in the case-hardened steel of conventional purity and CVT case-hardened steel with extra-pure specifications. As shown, the amount and magnitude of inclusions are smaller and the distribution curve does not have a foot. On the other hand, for surface-originating flaking, it is indispensable to eliminate the harmful nature of surface indentations from hard foreign debris. Many hard foreign particles are contained in the oil of differential gear boxes and rolling fatigue life under such conditions, in the worst case, may be shortened to 1/5 of the calculated life. The main reason for shortened fatigue life is stress concentrations around the edge of debris indentations. TF technology relieves such stress concentrations. Fig. 15 illustrates a debris dent and the stress concentrations around it. Stress concentration is expressed by the r/c value, which is the ratio of curvature of the edge of the indentation r and diameter of indentation, $2c$. It shows that the smaller the

Table 1 Prototypes of the half toroidal CVT

Year	1982	1983	1983	1983	1984	1985	1986
Name	T150S/SBR	T90S/SC	T90S/HM	T68S	T125S	T104S/DH	T116S
Engine	1 600 cc FF Car	550 cc Mini Van	400 cc Motorcycle	180 cc Motorcycle	2 000 cc Diesel Van	550 cc Turbo FF Mini Car	Motorcycle Motorcycle
Max. Power	63.75 Kw	22.5	30	9	49.5	39	73.5
Max. Input Torque	120.5 Nm	44.1	32.34	11.761	124.46	ÇV70.56	110.74
Max. Input Speed	5 600 rpm	5 500	10 000	8 500	4 500	6 000	7 000
CVT Ratio: Total	4.0	4.0	4.0	4.0	6.0	5.2	4.0
Reduction	2.0	2.0			2.449	2.280	2.0
Acceleration	0.5	0.5	0.5	0.5	0.408	0.438	0.5
Toroidal Specs.							
Cavity Formation	Single	Single	Single	Single	Single	Single	Single
Cavity Dia.	150 mm	90	90	68	125	104	116
Disc Dia.	165 mm	100	100	90	150	116	124
Traction Oil	Santotrac 50	Santotrac 50	DN 7073	DN 7074	DN 7074	DN 7088	DN 7074
CVT Control	Hydro-Mech.	Hydro-Mech.	Hydro-Mech.	Hydro-Mech.	Hydro-Mech.	Hydro-Mech.	Hydro-Mech.
Starting Clutch	Manual	Elect. POWDER Elect. Control	Manual	Centrifugal	Elect. POWDER	Wet Friction Plate/CPU	Centrifugal
Progress	Road Test: 20 000 miles US Highway Bench Test: Life, Efficiency	Road Test: Rough and Snow Road, City Road Bench Test: Life, Efficiency	Bench Test: Life, Efficiency	Road Test: City Road Bench Test: Life, Efficiency	Road Test: City Road	Road Test: Rough and Snow Road, City Road Bench Test: Life, Efficiency	Road Test: City Road and Highway Bench Test: Life, Efficiency

Year	1987	1988	1990	1992	1993	1994	1999
Name	T150S	T150D	T144D	T145D	T132D	T130D	T132D
Engine	1 500 cc TURBO FF Car	3 000 cc TURBO Bench	3 000 cc TURBO FR Car	3 000 cc rWD	4 000 cc FF Car	4 000 cc FR Car	3 000 cc TURBO FR Car
Max. Power	75	191.25	191.25	106.6			206
Max. Input Torque	156.8	333	333	230	370	340	387
Max. Input Speed	6 000	6 000	5 500	7 000	7 000	6500	
CVT Ratio: Total	5.6	5.6	5.6	8.7	4.0	5.2	4.4
Reduction	2.366	2.366	2.366	2.950	2.000	2.280	2.000
Acceleration	0.422	0.422	0.422	0.339	0.500	0.439	0.460
Toroidal Specs.							
Cavity Formation	Double	Double	Double	Double	Double	Double	Double
Cavity Dia.	150	150	150	145	132	150	132
Disc Dia.	165	165	165	165	155	165	158
Traction Oil	Ap. 7149	Ap.7149	Ap.7149	A.7149	A.7149	A.7149	Mass-Pro.Type
CVT Control	Hydro-Elect.	Hydro-Elect.	Hydro-Elect.	Hydro-Elect.	Hydro-Elect.	Hydro-Elect.	Hydro-Elect.
Starting Clutch	Torque Converter		Torque Converter				Torque Converter
Progress	Road Test: City Road Bench Test: Life, Efficiency	Bench Test	Road Test Bench Test	Bench Test	Bench Test: Efficiency	Bench Test: Efficiency	Mass-Production

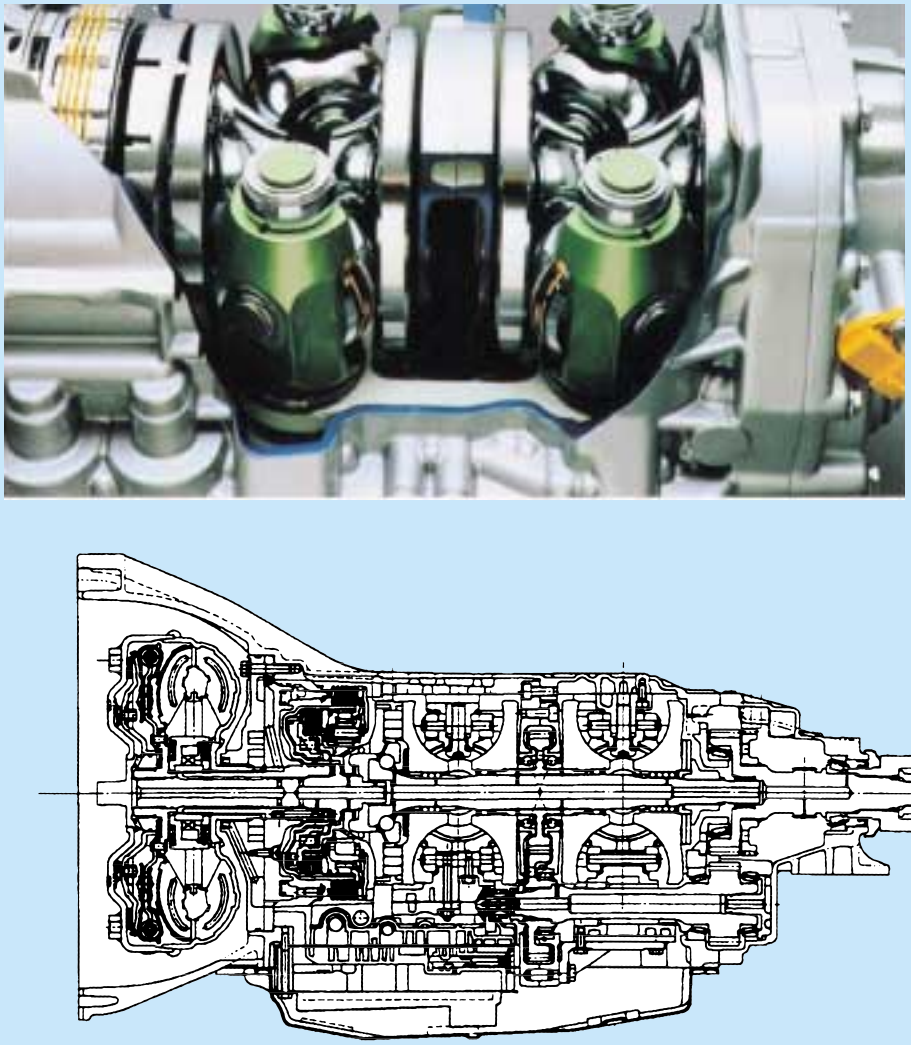

Fig. 19 Nissan Extroid CVT

r/c value, the larger the stress concentration. Fig. 16 shows the relation between *r/c* value and the amount of retained austenite. Essentially, TF technology involves raising the retained austenite content by heat treatment and thus increasing this *r/c* value. Rolling contact fatigue life test results are shown in Fig. 17. As the amount of retained austenite increases, fatigue life becomes longer. In addition, with the adoption of carbonitriding, it is possible to obtain the ideal material quality with a high retained austenite content while still achieving high hardness. Further, it is possible to realize long life under high temperature and high surface pressure by preventing deterioration of durability under high temperatures by applying a solid solution of nitrogen through carbonitriding. Fig. 18 shows endurance test results of the traction surface. During the period from 1984 to 1987, flaking occurred rather frequently, but after 1993, when CVT steel with carbonitriding began to be used, no flaking of the traction surface occurred and long fatigue life was achieved.

7. NSK Prototypes and Development History

Table 1 shows the development history of NSK prototypes. Early on, the focus of development was for small engines and experiments on endurance, efficiency and control were mainly conducted. Then, after 1987, we did not make complete prototypes, focusing our efforts instead on the disks and power rollers that have become the POWERTOROS UNIT. Finally, a photograph and cross-section of the CVT transmission installed in Nissan Motors' Cedric and Gloria are presented in Fig. 19.

References:
1) Kraus, Machine Design, Oct. 18, (1973), 20–24
2) Hamrock, B. J. and Dowson, D., Trans. ASME, J. Lubr. Technol., 99–1(1977), 15
3) Johnson, K. L. and Tevaarwerk, J. L., Proc. R. Soc., London, Ser. A, 356 (1977), 215–236
4) Tevaarwerk, J. L. and Johnson, K. L., Trans ASME, Ser. F, 101–3 (1979), 266–274
5) Evans, C. R. and Johnson, K. L., Inst. Mech. Eng., C5 (1986) 303–312
6) Evans, C. R. and Johnson, K. L., Inst. Mech. Eng., C5 (1986) 313–324
7) Tanaka, H., Journal of JSME, 53–491, C (1987), 1500 [in Japanese]
8) Achiha, H. and Natsumeda, S. et al, Proc. ITC Yokohama 1995, JAST, 139–144
9) Tanaka, H. and Furumura, K., SAE paper 830570 (1983)

Hisashi Machida

Yasuo Murakami

Recent Developments in Highly Precise NSK Linear Guides

Soichiro Kato and Jun Matsumoto
Precision Machinery & Parts Technology Center

1. Introduction

Recently, demand for enhanced accuracy of rolling linear guides is increasing in response to remarkable improvements in the accuracy of machine tools and other manufacturing and inspection equipment in which linear guides are installed.

Key factors that adversely affect the motion accuracy of linear guides are cyclic displacement of the ball slide due to ball passage and deflection of the rail caused by tightening bolts. In this report, we describe our research on these two factors and then present measures for improving the accuracy of linear guides.

2. Motion Accuracy of Linear Guide

The test rig shown in Fig. 1 was used to assess the accuracy of a linear guide consisting of one rail and one ball slide. Changes in the posture (angle) of the linear guide were measured by an automatic collimator as the ball slide moved at a constant speed. Results are shown in Fig. 2. Two noteworthy fluctuation components were observed:

(1) Ball passage vibration

The short-wavelength fluctuation component seen in Fig. 2 is related to the movement of the balls inside the linear guide and it is called ball passage vibration. The wavelength of fluctuation is approximately double the ball diameter.

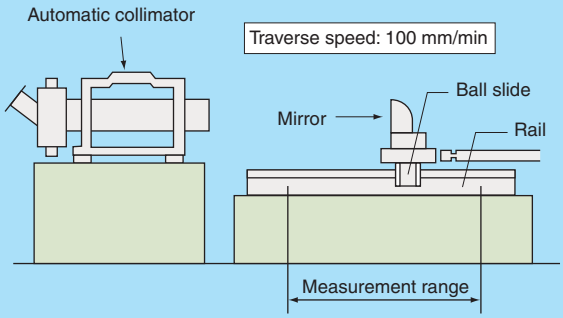

Fig. 1 Method for measuring the motion accuracy of an NSK linear guide

(2) Fluctuation of bolt pitch

The wavelength of the longer fluctuation component seen in Fig. 2 is nearly equal to the pitch of the linear guide's mounting bolts. This fluctuation is caused by deflection of the rail by tightening bolts.

3. Suppression of Ball Passage Vibration

3.1 Measurement of ball passage vibration

Ball passage vibration measurements taken using the test rig in Fig. 1 are shown in Fig. 3. Vibration of a wavelength about double the diameter of the ball is

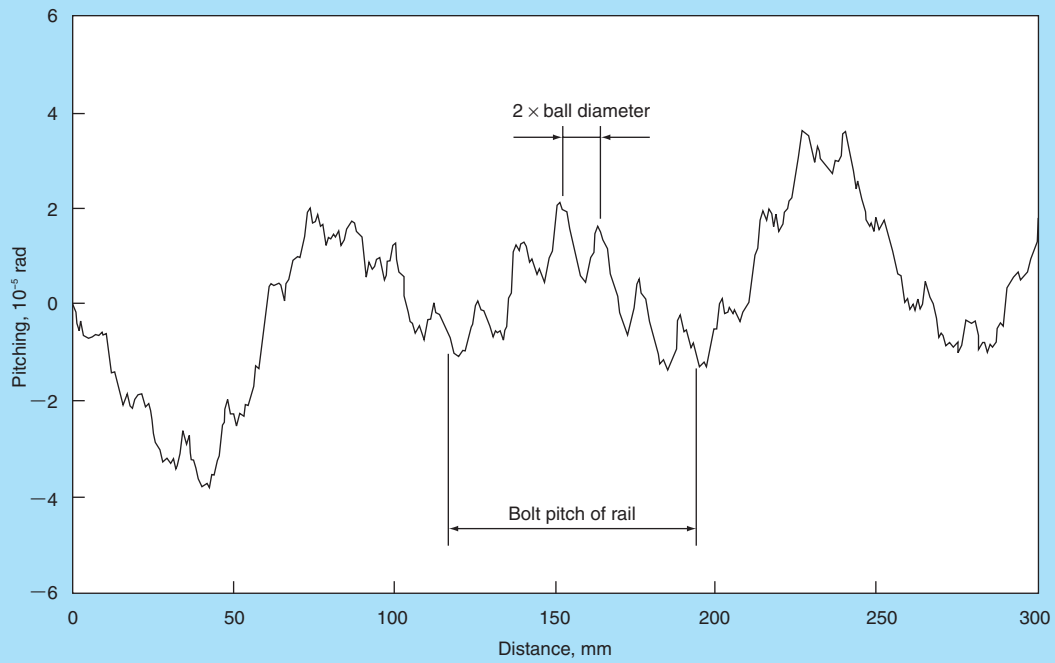

Fig. 2 Motion accuracy of an NSK linear guide

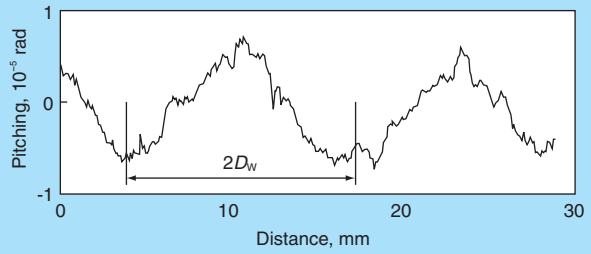

Fig. 3 Example of vibration caused by ball passage
(Ball diameter D_w = 6.35 mm)

observed. While the angular fluctuation of the ball slide caused by ball passage vibration is small, it is amplified to large displacement at the overhang point (position far from the ball slide) and therefore often becomes a problem.

3.2 Mechanism of ball passage vibration

To explain the mechanism of ball passage vibration simply, we will use the linear guide with two rows of ball grooves shown in Fig. 4(a). We suppose that the arrangement of the balls in the two grooves is staggered as shown in Fig. 4(b). As such, there are fewer balls in the upper groove than the lower one. If the linear guide is preloaded and no external load is applied, the load on the balls in the upper groove is equal to the load on the balls in the lower groove. Consequently, the load on one ball in the upper groove is greater than the load on one ball in the lower groove, which means that the balls in the upper groove are deformed more than those in the lower groove. Compared to when the arrangement of balls in the upper and lower grooves is the same (Fig. 4(a)), the ball slide moves downward. From this state when the ball slide travels by D_w, the balls move by $D_w/2$ and the state becomes that shown in Fig. 4(c). In this case, the arrangement in Fig. 4(b) is switched so that, compared to the arrangement in Fig. 4(a), the ball slide moves upward. When the ball slide travels a distance twice that of the ball diameter, the balls return to their original state. Therefore, fluctuation repeats at intervals equal to twice the ball diameter. This is the major reason for ball passage vibration.

While the preceding discussion concerned linear guides with two ball grooves, a similar way of thinking is applicable for linear guides with four ball grooves like the one in Fig. 5(a). Additionally, while here we discussed only vertical displacement, for similar reasons, the ball slide also moves in horizontal and rotational directions, i.e., pitching, yawing and rolling directions.

For a linear guide with four ball grooves, it is theoretically possible to calculate the posture change in all directions by supposing the arrangement of the balls in each groove and thinking the balance of its whole force and load moment. However, with such a method, the equation becomes troublesome. In section 3.3, we present a simplified calculation method with which the maximum value of ball passage vibration can be obtained.

Taking the up, down and pitching directions as representative, ball arrangement is assumed to be the

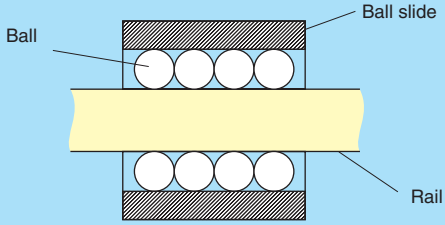

(a) Model of linear guide with two grooves

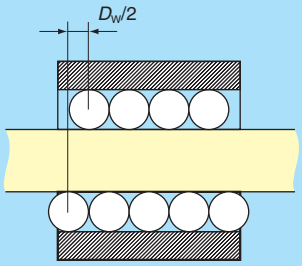

(b) Position of balls in upper and lower grooves

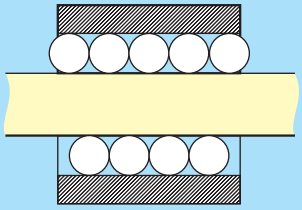

(c) Position of balls after traveling $D_w/2$
(Ball slide moved by D_w from their position in (b))

Fig. 4 Mechanism of vibration caused by ball passage

same in grooves 1 and 2 and in grooves 3 and 4 in Fig. 5(a). The balls in grooves 1 and 3, and 2 and 4, respectively, are assumed to be staggered by half of the ball diameter (more exactly, the distance between the ball centers). The maximum value of posture change in the up, down and pitching directions can be calculated.

Also, for other directions calculation of posture change is possible with similar thinking. For the right, left and yawing directions, it can be obtained by assuming that the ball arrangement is the same in grooves 1 and 3 and in grooves 2 and 4, and for the rolling direction, by assuming that the ball arrangement is the same in grooves 1 and 4 and in grooves 2 and 3 in Fig. 5(a).

3.3 Calculation of ball passage vibration

In the preceding section, for the purpose of simplification, we assumed that the ball grooves had a uniform cross-sectional shape in the longitudinal direction. In fact, however, as shown in Fig. 5(b), the end of the ball groove has a gently slanting curve called crowning. Thanks to crowning the load on a ball at the end of the ball slide gradually increases or decreases as it travels and posture change of the ball slide is also relieved. Here we show the theoretical calculation method for ball passage vibration taking into account the effect of crowning.

Let's consider the linear guide with four ball grooves shown in Fig. 5(a). All four grooves have the same shape and their length is L_1. The contact angle (α), displacement

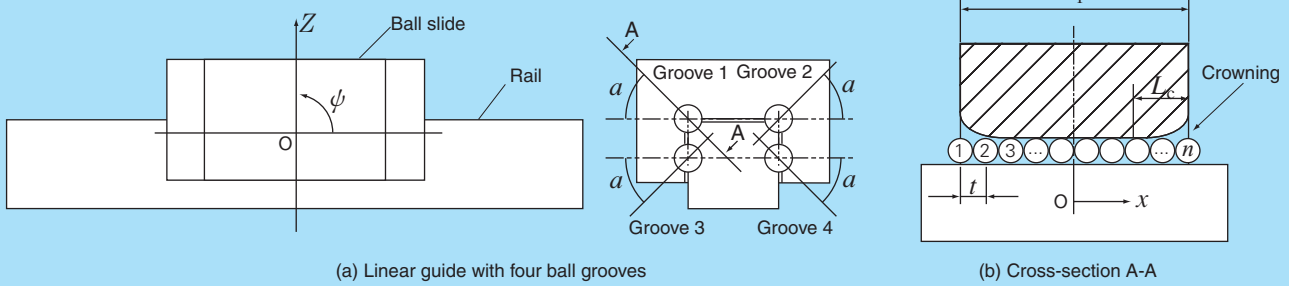

(a) Linear guide with four ball grooves (b) Cross-section A-A

Fig. 5 Linear guide construction

in up/down direction (z), and angular change in the pitching direction (ψ) are as shown in the figure. Fig. 5(b) is a cross-sectional view of the upper ball groove cut by the plane parallel to the contact angle (A-A cross-sectional view of Fig. 5(a)). Balls are assumed to be arranged with the fixed distance t between their centers, and the balls are numbered consecutively from left to right $i = 1, 2, 3, \ldots n$. The center of longitudinal direction of the ball slide is fixed as the origin, and coordinate axis X is fixed along the ball groove. When the x coordinate of the center of ball 1 is set as x_1 ($-L_1/2 \leq x_1 < t - L_1/2$), the coordinates of x_i of the center of the ith ball is given by this equation:

$$x_i = x_1 + (i-1)\,t \quad \ldots\ldots (1)$$

When posture change of the ball slide occurs by Δz in the up/down directions, and by $\Delta\psi$ in the pitching direction, the elastic deformation of ith ball δ_i is calculated by this equation:

$$\mathrm{d}_i = \mathrm{d}_o - \mathrm{D}z \sin\alpha - x_i \cdot \mathrm{D}\psi \sin\alpha + \mathrm{d}_{CRi} \quad \ldots\ldots (2)$$

However, if d_i becomes less than 0, d_i is set to equal 0.

Here, d_o is the elastic deformation of the balls caused by preload. d_{CRi} is the elastic deformation (zero or a negative value) of the balls caused by crowning. If the crowning is an arc within the horizontal plane, d_{CRi} can be calculated by Equation (3), setting the crowning radius as R and the crowning length as Lc.

$$\delta_{CRi} = \begin{cases} -\dfrac{\left(x_i + \dfrac{L_1}{2} - L_c\right)^2}{2R}\cos\alpha & \left(-\dfrac{L_1}{2} \leq x_i < L_c - \dfrac{L_1}{2}\right) \\ 0 & \left(L_c - \dfrac{L_1}{2} \leq x_i \leq \dfrac{L_1}{2} - L_c\right) \\ -\dfrac{\left(x_i - \dfrac{L_1}{2} + L_c\right)^2}{2R}\cos\alpha & \left(\dfrac{L_1}{2} - L_c \leq x_i < \dfrac{L_1}{2}\right) \end{cases} \quad \ldots\ldots (3)$$

The ball load to the ith ball, Q_i, is given by this equation:

$$Q_i = K\,\mathrm{d}_i^{3/2} \quad \ldots\ldots (4)$$

Here, K is a constant determined by the design of the ball groove.

Similarly, x coordinates of the center of a ball in the lower groove and the ball's load are indicated by affixing an apostrophe (′) to the respective symbols. The balance of force and moment of the ball slide is expressed by Equations (5) and (6) below.

$$\sum_{i=1}^{n} Q_i = \sum_{i=1}^{n} Q_i' \quad \ldots\ldots (5)$$

$$\sum_{i=1}^{n} x_i Q_i = \sum_{i=1}^{n} x_i' Q_i' \quad \ldots\ldots (6)$$

Using Equations (1) through (6), posture change (Δz and $\Delta\psi$) can be obtained. In practice, one calculates numerical values of Δz and $\Delta\psi$ that make Equations (5) and (6) valid. Taking the coordinates of the center of a ball at the left end x_1 as a parameter, by calculating Δz and $\Delta\psi$, the relation between traveling distance of ball slide and posture change can be calculated.

We have presented here the calculation method for the up/down and pitching directions. As stated in the previous section, similar calculations can be performed for the right/left, yawing and rolling directions.

3.4 Comparison of measured and calculated values

An example of calculation results of the up/down and pitching directions when the ball arrangement in the upper and lower grooves is staggered by 1/2 of t, the distance between ball centers, is shown in Fig. 6. Vibration with a wavelength about twice the ball diameter (more exactly, twice the distance between ball centers) is observed. Measured and calculated values of ball passage vibration for several kinds of linear guides are compared in Fig. 7.

While as stated above the calculated value is the maximum value, the maximum measured value is taken from among several repeated measurements. The measured values matched well with the calculated values and the effectiveness of the proposed calculation method was thus confirmed.

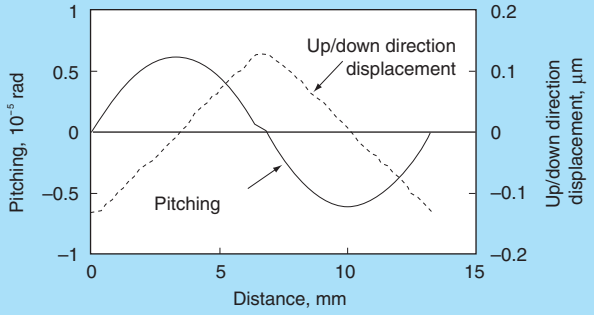

Fig. 6 Calculation example: Vibration caused by ball passage (Ball diameter D_w = 6.35 mm, medium preload)

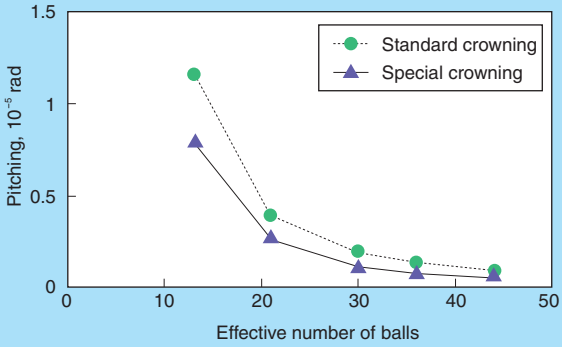

Fig. 8 Effective number of balls and calculated vibration by ball passage (Ball diameter D_w = 4.76 mm, medium preload)

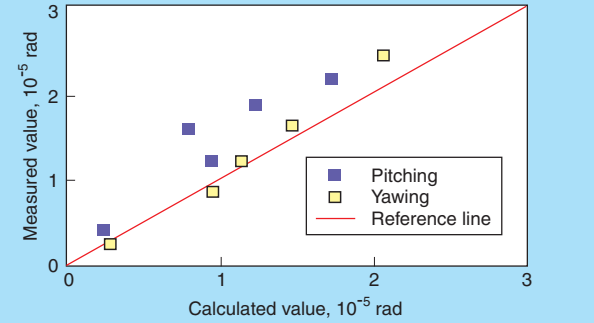

Fig. 7 Comparison of actual and calculated vibration

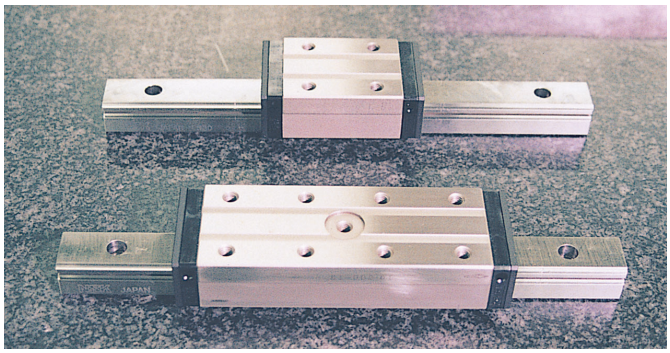

Photo 1 NSK linear guide with super-long ball slide (front side)

3.5 Effect of super-long specification

Due to the structure of linear guides, vibration from ball passage is unavoidable, even if a product is geometrically correct. However, such vibration can be relieved through effective design. Here we discuss our design guidelines for suppressing ball passage vibration.

Fig. 8 shows the relation between a) the number of rolling elements sustaining the load per groove ("effective number of rolling elements") when the elastic deformation of balls caused by the preload is constant and b) values of ball passage vibration calculated based on the method described in section 3.3. Calculations were performed for two types of crowning: standard crowning and special crowning with a larger radius. The results indicate that increasing the effective number of rolling elements and applying the special crowning suppress ball passage vibration.

Based on this result, we developed linear guides with a super-long specification for which the effective number of balls is double or triple that of standard-length linear guides and special crowning is applied. Photo 1 shows a

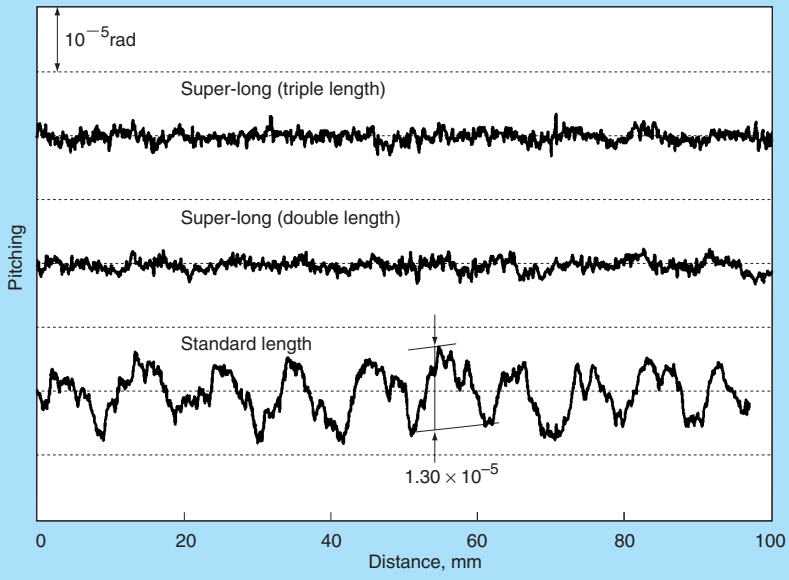

Fig. 9 Vibration caused by ball passage in linear guide with super-long ball slide (Ball diameter D_w = 4.76 mm, medium preload)

linear guide of the super-long specification.

The motion accuracy of both a super-long and standard linear guide with one rail and one ball slide was measured by the method shown in Fig. 1. Results are compared in Fig. 9. With the standard length, significant ball passage vibration was observed, while with the super-long specification of both double and triple length, nearly no fluctuation was observed. These results clearly indicate that the super-long specification is an effective means of suppressing ball passage vibration.

4. Rail Accuracy Improvement

4.1 Deflection of rail by bolt tightening

The rail of a linear guide is tightened and fixed to the base component by bolts. Naturally, the rail is an elastic body and the compression force generated by tightening the bolts causes its deflection. The broken line in Fig. 10 simulates this deflection. Compromising motion accuracy, the rail deforms wavily in a longitudinal direction corresponding to the bolt pitch.

NSK grinds the rail after having fixed it under a specified torque. When the linear guide is actually used, the bolts are tightened with the same tightening torque to reproduce the groove accuracy present during groove grinding. Through this practice, most of the accuracy error caused by rail deflection can be eliminated.

Still, even if the bolts are tightened with the specified torque, error or dispersion of their compression force (axial tension of bolts) occurs due to differences in the friction coefficients of the bolts (lubrication conditions of the seat faces and threads of the bolts). Even if tightening is error-free, because the hardness and cross-section coefficient of the base when the groove is ground are different from when the linear guide is actually used, perfect reproduction is impossible. Therefore, for highly precise applications, rail deflection must be minimized, even if errors occur in the amount of compression force applied when tightening the bolts or if there are differences in the characteristics of the linear guide's base.

4.2 Analysis of deflection and the effectiveness of countermeasures

To determine the best method for suppressing rail deflection caused by bolt tightening, at first we surveyed the way in which rails are deflected in the vertical direction.

The relation between rail position and deflection

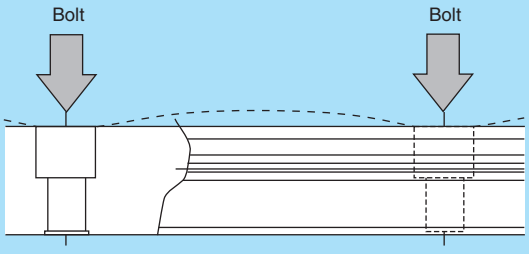

Fig. 10 Model of rail deflection

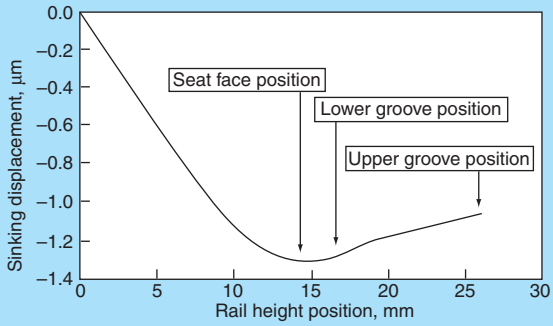

Fig. 11 Relation between deflection and position on rail using FEM

(sinking) amount caused by bolt tightening was analyzed through FEM analysis. The results are shown in Fig. 11. For this analysis we chose NSK linear guide LH30. On both sides of the rail two upper and lower ball grooves are ground. The standard calls for the seat face of the bolt hole to be a little lower than the center of the lower groove. From Fig. 11 it became clear that greater deflection occurs in the area lower than the bolt seat face and that the maximum deflection occurs near the lower groove, close to the seat face. Based on this result, we decided to analyze the effect of making the counter bore of the bolt holes deeper.

While it is assumed that the deeper the counter bore the more effective it is in reducing deflection, due to limits imposed by strength considerations, we decided to determine the counter bore depth through strength analysis. Through strength analysis by FEM, we determined that the basic static load, which is the permissible maximum load of the linear guide, is applied to the direction to detach the rail from the base. The load application point was set at the center of the span between bolts and it was supposed that the load was sustained by only two bolts on both its sides.

We calculated the relation between the counter bore depth of the bolt holes and the maximum stress on the root part of the seat face and we considered this relation with regard to material strength. Based on these results and the results of experiments described later, we decided to make the counter bore deeper, increasing from the standard of 12 to 18 mm, while allowing a sufficient margin for safety.

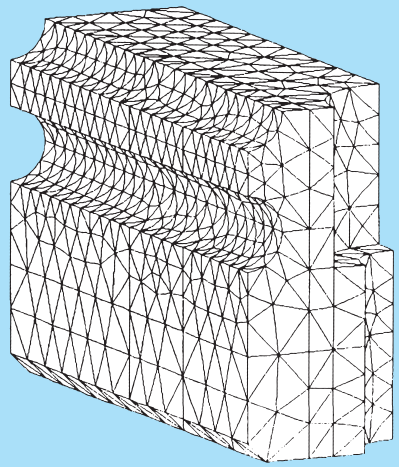

Fig. 12 FEM model of linear guide rail

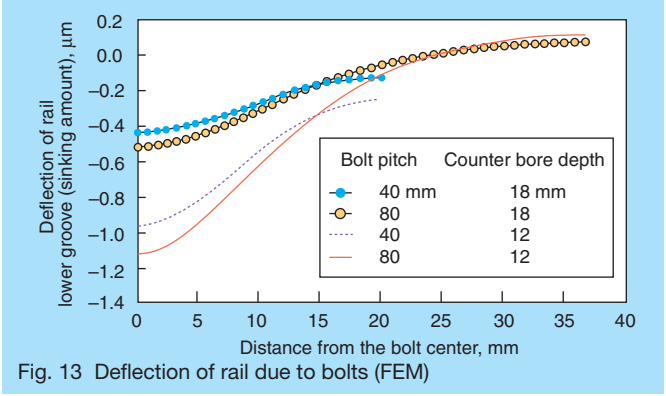

Fig. 13 Deflection of rail due to bolts (FEM)

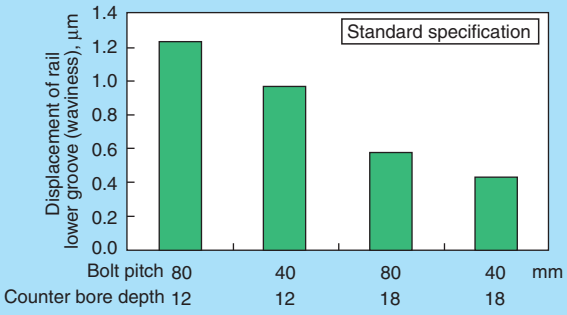

Fig. 14 Effect of counter bore depth and bolt hole pitch on rail deflection

In testing of a rail with 18-mm-deep counter bores, we confirmed that the bolts only break before the rail seat face when a load exceeding the basic static load is applied. The reliability of these results is bolstered by the fact that the number of bolts sustaining the load in actual conditions is much greater than the two considered in the FEM analysis.

Additionally, because deflection (waviness in the longitudinal direction) is reduced by increasing the constraint points (shortening the bolt pitch of the rail), we decided to adopt this measure as well.

4.3 Analysis and experiments on the effectiveness of countermeasures

First, we explain about the FEM analysis conducted to evaluate the effectiveness of the countermeasures. Fig. 12 shows an FEM model of the rail of an LH30 linear guide with standard specifications. Fig. 13 shows the deflection of rails at the lower groove with differing bolt pitches and counter bore depths. Fig. 14 shows the maximum deflection values of the various rails in Fig. 13. As shown in Fig. 14, deflection is reduced by more than half of the conventional specification by deepening the counter bore from 12 to 18 mm. Further, by shortening the bolt pitch from 80 to 40 mm, deflection is cut by an additional 20%. Combining these measures, deflection is reduced by 2/3 approximately.

Next, we present the results of an experiment conducted to confirm the effect of these measures on the motion accuracy of the linear guide. In the tests, we used two LH30 linear guides. One had a counter bore depth of 12 mm (standard) and the other, 18 mm. Bolt pitch was standard. The results shown in Fig. 15 were obtained using the method illustrated in Fig. 1 under the following conditions:

Test linear guide: LH30 super high load type, medium preload
Measurement speed: 4 mm/sec
Measurement stroke: 380 mm

As shown in Fig. 15, it was confirmed that the motion accuracy was greatly improved. The waviness component of the bolt pitch observed with the rail with the standard 12 mm counter bore depth was not observed with the rail with the 18 mm counter bore.

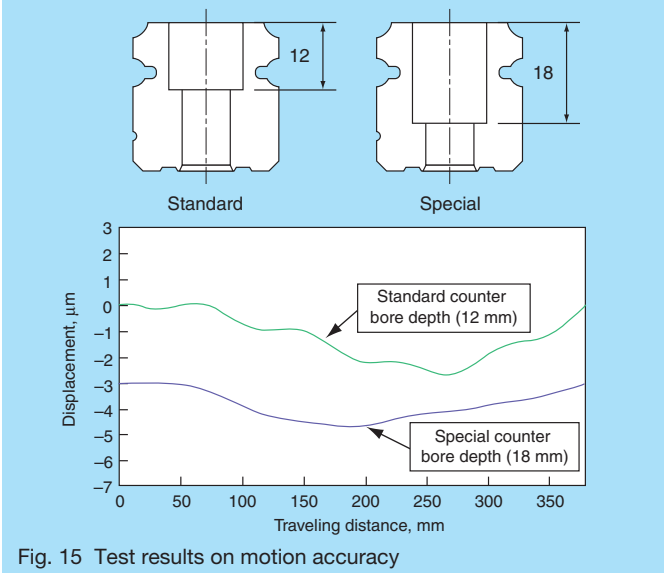

Fig. 15 Test results on motion accuracy

5. Conclusion

We examined theoretically and experimentally the influence of ball passage vibration and rail bolt tightening on the motion accuracy of linear guides. The efficiency of measures for improving precision was confirmed and a method for estimating the effect of these measures through calculation was developed.

In response to the increasing demand for higher precision, we will continue our efforts toward establishing the optimal design for suppressing motion accuracy error.

Soichiro Kato

Jun Matsumoto

Molded-Oil™ Bearings

Molded-Oil™ Bearings (Photo 1) are lubricated with NSK's own oil-impregnated material, Molded-Oil™. This outstanding new material consists of lubricating oil and polyolefin resin that has an affinity for oil. Oil slowly seeping from this material provides ample lubrication to bearings for extended periods.

Features

■ Excellent performance in water- and dust-contaminated environments

Bearing life under contaminated lubrication is extended because the lubricant is resistant to both water and dust.

■ Environmental compatibility

As oil seeping from the Molded-Oil™ inside the bearing provides sufficient lubrication, troublesome oil refilling is not required and contamination of the surrounding environment is prevented.

■ Low torque

The interior surfaces of the bearings are specially treated prior to filling with Molded-Oil™. As a result, bearing torque is not much higher than that of grease-lubricated bearings. (Patent pending)

Applications

Applications for Molded-Oil™ Bearings include:

- Steel mill equipment
- Food processing equipment
- Liquid crystal and semiconductor manufacturing equipment
- Agricultural machines
- Cleaning equipment and lines
- Material-handling and conveying equipment
- Production lines and machines for which maintenance is difficult

Photo 1 Molded-Oil™ Bearings

Availability

■ Temperature range (outer ring): -15 to 80°C

■ Bearing types, sizes and limiting speeds

$d_m n$ = (Bearing bore diameter, mm + Bearing outside diameter, mm) ÷ 2 × Rotational Speed, rpm

The limiting speeds reflect that the internal space of the bearings is completely filled with Molded-Oil™.

Regarding bearing numbers and other bearing types, please contact NSK.

Bearing type	Maximum available outside diameter, mm	Limiting speed, $d_m n$, mm • rpm
Spherical roller bearings	250	60 000
Deep groove ball bearings	250	150 000

Performance

Test data and field results demonstrate the outstanding performance of Molded-Oil™ Bearings.

■ Durability test under water exposure

In wet conditions, Molded-Oil™ Bearings have longer life than grease-lubricated bearings. (Fig. 1)

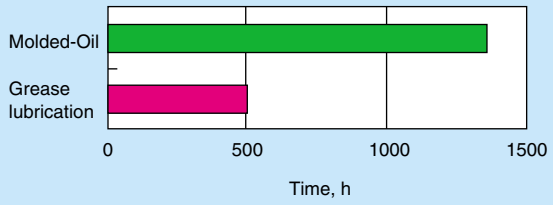

Test conditions

Test bearings:	6000 (stainless steel, with seals)
Rotational speed:	1 000 rpm
Radial load:	78.4 N
Axial load:	29.4 N
Water exposure:	0.8 cm³/min (1 cycle = 1 sec, spray + 9 sec, no spray)
Spray pressure:	0.2 MPa

Fig. 1 Results of durability tests under water exposure

Extra-Capacity Sealed-Clean™ Roll Neck Bearings

NSK, the first in the world with sealed roll neck bearings, delivers again with Extra-Capacity Sealed-Clean™ Bearings for roll necks. (Photo 1, Fig. 1)

Photo 1 Extra-Capacity Sealed-Clean™ Roll Neck Bearings

Features

- Prevention of water entry
- Increased load capacity
- Easier handling
- Greater durability under severe lubrication conditions

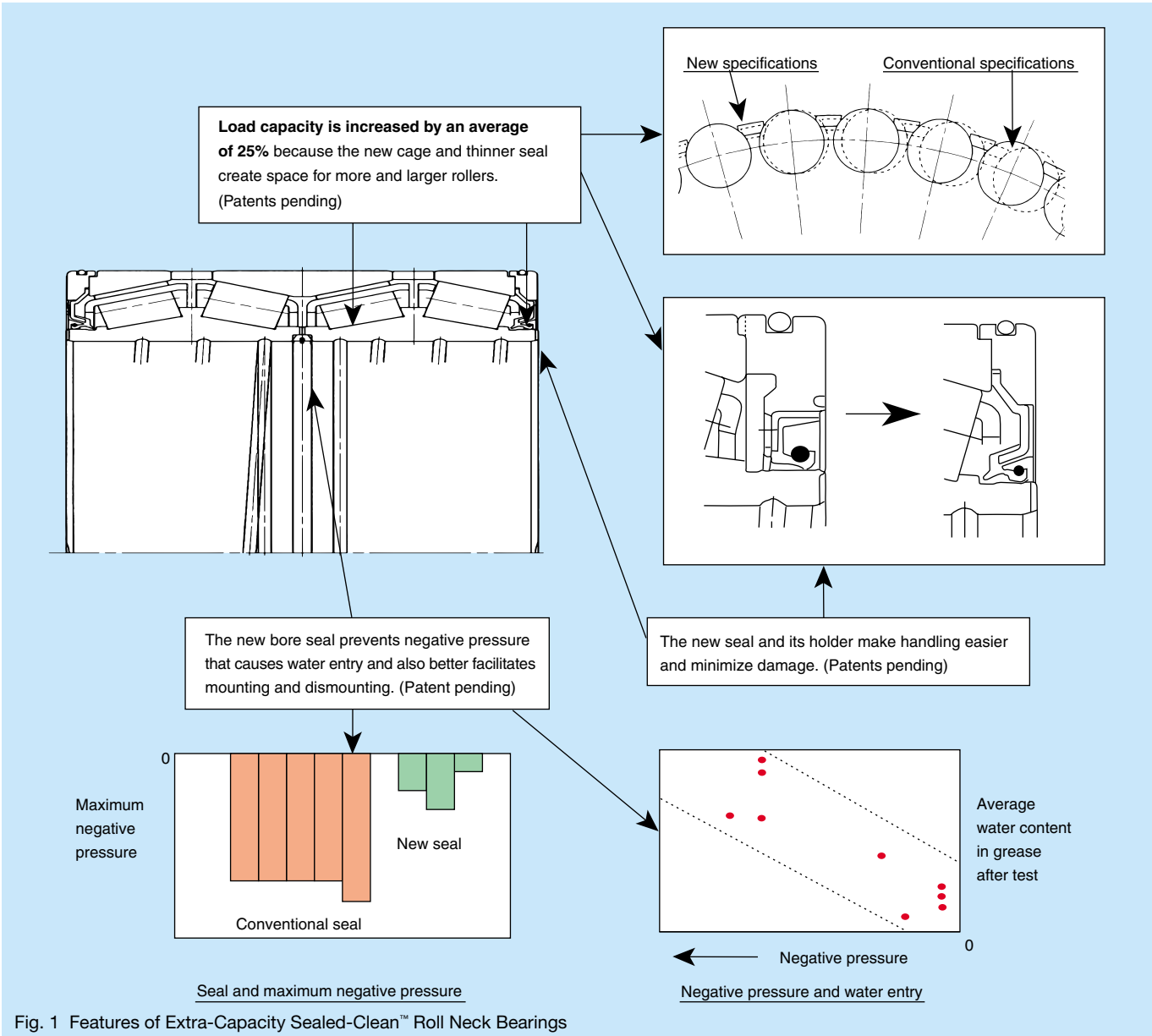

Fig. 1 Features of Extra-Capacity Sealed-Clean™ Roll Neck Bearings

Double Cardan Constant-Velocity Universal Joint (Double Cardan Joint)

In response to tighter collision safety standards (including raising the head-on collision speed from 40 to 50 km/h) enacted in October 1998 for mini-sized motor vehicles (660 cc or fewer), manufacturers made extensive design changes. In the course of improvement efforts, cases arose where the conventional layout of the intermediate shaft assembly with two joints did not ensure adequate safety in the event of a head-on collision. To solve the problem, NSK developed a double Cardan constant-velocity universal joint.

Requirement for Double Cardan Joint

The steering system of a car generally has two joints that are linked. The use of air bags to improve safety means that the steering column must be arranged at a smaller inclination in order to withstand the reactive force of the air bag in the event of its deployment. As a result, the angles of joints 1 and 2 in Fig. 1 need to be equal to ensure smooth transmission of the steering wheel rotation. However, this is unfeasible with existing car designs, as this arrangement is possible only when joint 2 is positioned outside the car. While arrangement is possible if the body is extended at the front end or if the steering gear system can be shifted backwards, this would require sacrificing trunk space and diminish the commercial value of the car. NSK's double Cardan constant-velocity universal joint, which appears to be only one joint, has solved this problem.

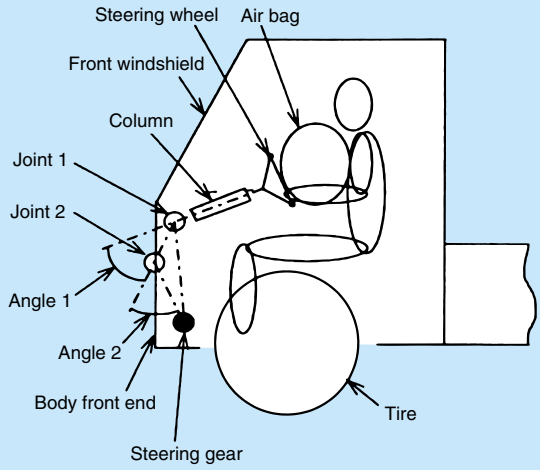

Fig. 1 Layout necessitating NSK's double Cardan joint

Construction

The construction of the double Cardan constant-velocity universal joint basically features two Cardan joints that are synchronized to maintain an equal joint angle and assembled in one package to cancel the change in torque.

■ Types

There are two types of double Cardan constant-velocity joints: a one-ball type with a joint angle between 0 and 40 degrees and a twin-ball/center-plate type with a joint angle between 0 and 70 degrees. NSK's double Cardan joint is the twin-ball/center-plate type.

■ Principle

For the two joints to maintain equal turning speed, it is essential that they be arranged so that they rotate while maintaining the central constant-velocity plane between them (Fig. 2). Our double Cardan joint is based on this principle.[1)]

■ Actual construction

The crank turns on both sides of the center plate, which serves as a bearing. The sleeve (united with the crank) and the ball at the end of the forged yoke are engaged with each other to keep the angles of the two joints equal. Constant velocity is maintained through this mechanism. (See Fig. 3.)

The surfaces and parts that are in sliding contact with the crank greatly affect the durability of the joint. We have achieved high durability by employing a resin bush (made of polyoxymethylene, POM; brand name: Tenac®).

The appearance of double Cardan joint is shown in Fig. 4.

Features

■ Pressed center yoke

Significantly reducing costs, the center yoke is now pressed instead of forged.

■ Sintered crank

To save machining work and reduce costs, the crank is made of a sintered metal.

■ Resin bush

Employing the resin bush described above ensures sufficient durability.

■ Needle bearing employed for support of metal bottom

A large secondary moment is produced due to the short distance between the two joints. Therefore, the bottom support of a thrust piece type cannot sufficiently bear this moment load. For this reason, an arrangement that creates direct contact between bearing cups and spider spokes is employed.

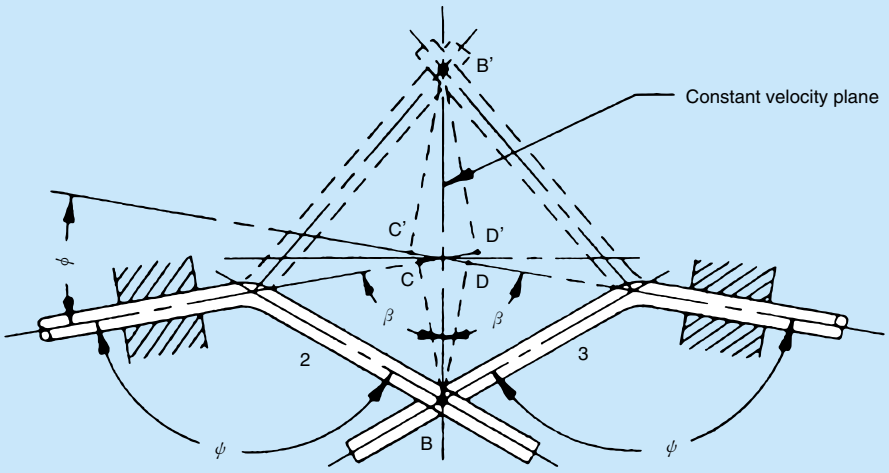

Fig. 2 Principle of constant velocity universal joint [1)]

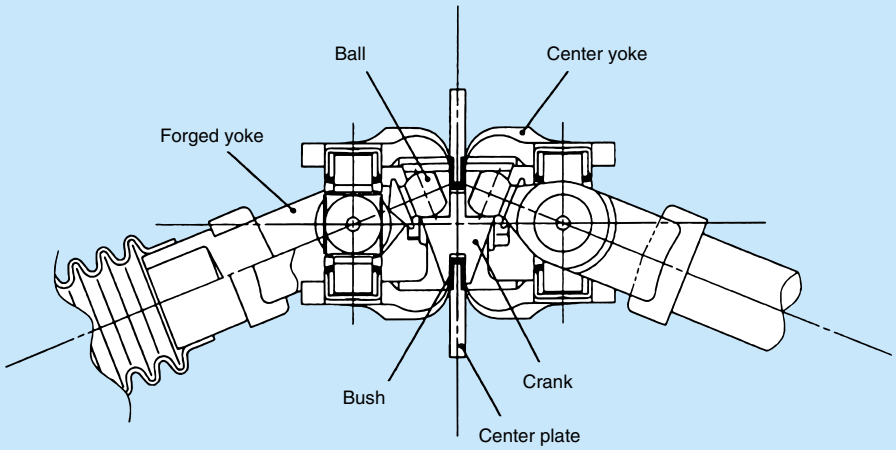

Fig. 3 Structure of double Cardan joint

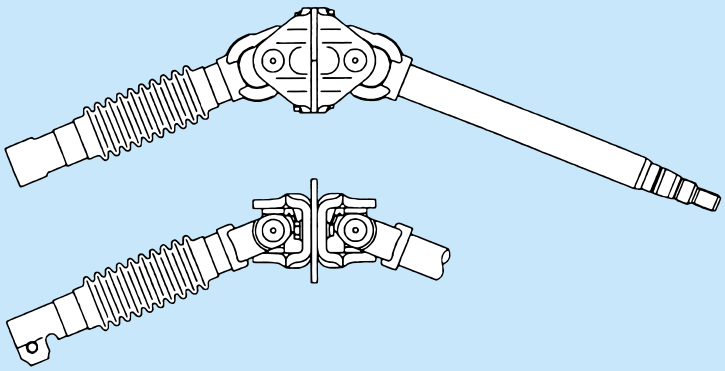

Fig. 4 Appearance of double Cardan joint

Conclusion

The development of this durable new product is the result of the efforts of many people in various fields. Work is ongoing at NSK to achieve further cost reductions and strengthen the feasibility of this product.

Reference:

1) SAE: "Universal Joint and Driveshaft Design Manual," Advances in Engineering Series, No. 7 (1979), 99

WFA Standard-Stock Ball Screws

NSK's MF (Maintenance-Free) Series of ball screws, linear guides and other products with compact, efficient NSK K1™ lubrication units have been well received in many industrial sectors. This article reports on a new addition to the MF Series, the WFA standard off-the-shelf ball screws (Photos 1 and 2).

Photo 1 WFA ball screws

Photo 2 WFA ball screw with NSK K1™ lubrication unit

What Are NSK K1™ Lubrication Units?

Recent market requirements of ball screws and linear guides are for reduced maintenance and the prevention of environmental pollution. While ball screws and linear guides are generally lubricated by forced intermittent oil or grease, these lubrication methods have their respective problems. Forced intermittent oil lubrication wastes a large amount of lubricating oil, requires costly piping and equipment, and causes contamination of the environment. Grease lubrication requires periodic replenishment, i.e., maintenance, and also can be rapidly deteriorated in harsh operating environments. In response, NSK developed NSK K1™ lubrication units. NSK K1™ lubrication units are made of "Molded-Oil," a special material developed by NSK consisting of lubricating oil and a plastic substance. A pair of NSK K1™ lubrication units, one on either side of the grease-packed nut of a ball screw or on either end of the ball slide of a linear guide, can supply lubricating oil at an optimum rate over a long period of time to the sliding surfaces and adjacent areas.

Features

Features of MF Series ball screws

Fitted with NSK K1™ lubrication units, MF Series ball screws have the following features:

■ Maintenance-free performance over a long period

NSK K1™ used in combination with grease provides efficient lubrication over extended periods to machine parts that are not easily accessible.

■ No contamination of surrounding environment with oil

When contamination from lubricating oil must be avoided to maintain cleanliness, NSK K1™ and a small quantity of grease provide sufficient lubrication.

■ Durability in applications exposed to water

Even in machines or equipment directly exposed to weather or subject to occasional wash-downs, NSK K1™ in combination with grease ensures a long service life.

■ Durability in environments where dust and debris impair lubrication

In operating environments where dust and debris absorb lubricating oil or grease, NSK K1™ in combination with grease provides effective lubrication for extended periods as well as limits the ingress of foreign particles.

Features of WFA ball screws

In addition to the features of the MF Series, WFA ball screws have the following features:

■ Fast delivery

WFA ball screws are readily available for delivery as standard-stock items and they come complete with their shaft ends ready for installation.

■ Low price

WFA ball screws are available at low prices equivalent to those of standard-stock A-Series ball screws that are not fitted with NSK K1™ lubrication units.

Table 1 Availability of WFA ball screws

Unit: mm

Shaft dia. × Lead / Stroke (nominal)	ϕ10 × 4	ϕ12 × 5	ϕ12 × 10	ϕ15 × 10	ϕ15 × 20	ϕ20 × 10	ϕ20 × 20
80	○	○	○				
190	○				○		
210				○			
230		○	○				
290	○						
400						○	
430		○	○				
600				○	○		○
700						○	
1 000				○	○		○
1 200						○	
1 400							○

Note: Detailed shapes and dimensions of WFA ball screws are listed in NSK catalog no. E3220 (1999 J-6).

Specifications

- WFA ball screws have an NSK K1™ lubrication unit on either side of the nut. The overall nut length of WFA ball screws is therefore about 20 to 30 mm longer than conventional ball screws without NSK K1™.
- Lubrication is provided by a combination of grease pre-packed in the nut and NSK K1™ lubrication units.
- The accuracy grade is JIS Grade C5 and clearance is eliminated by preloading.

Availability

WFA ball screws are available in the 21 combinations of screw shaft diameter, lead and nut stroke (nominal) listed in Table 1. The stroke (nominal) figures in the table are rounded-down values of possible travel distances of the nut on the screw shaft.

Applications

WFA ball screws are used extensively in a broad range of machinery, equipment and systems including, but not limited to:

- Semiconductor and liquid crystal display manufacturing machinery and equipment
- Robots and related systems
- Woodworking machinery
- Machine tools
- Automotive-related manufacturing facilities

Conclusion

NSK has developed various combinations of ball screws and NSK K1™ lubrication units that have already been widely distributed in the market. NSK will continue developing products that meet the expanding needs of the market.

High-Performance Seals for NSK Linear Guides

Linear guides are often operated in dusty environments where wood particles, rubber particles, graphite powder, ceramic powder or other dry materials are present in the air. For this reason, linear guides must have high sealing performance. NSK has recently developed high-performance side seals that provide better protection from outside contaminants than conventional seals. This article presents NSK's new long-life high-performance side seals.

Construction

A key feature of the new high-performance side seal is that part of the seal protrudes forward and has three lips to better keep out foreign inclusions and retain the grease within the ball slide (Fig. 1). Linear guides equipped with the new side seal have no wire groove in the rail for guiding a ball-retaining wire like conventional linear guides do. The new side seal reflects a priority for higher sealing performance and lower cost over ball retaining function during linear guide disassembly. Additionally, durability and sealing are enhanced by employing NSK K1™ lubrication units as standard in combination with the new side seal. Photo 1 shows a linear guide equipped with the new high-performance side seals and NSK K1™ lubrication units.

Photo 1 NSK linear guide equipped with high-performance side seal

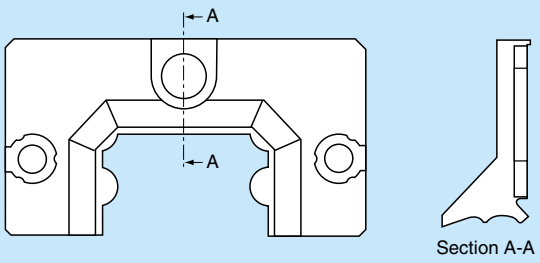

Fig. 1 Structure of new high-performance side seal

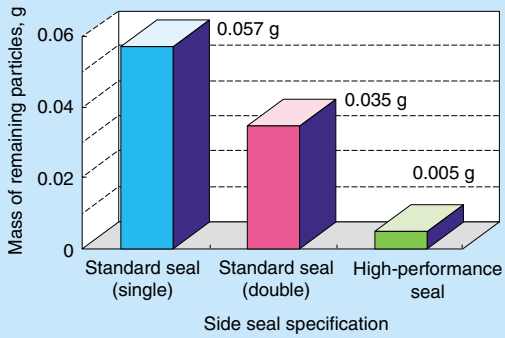

Fig. 2 Mass of particles remaining on rail after test

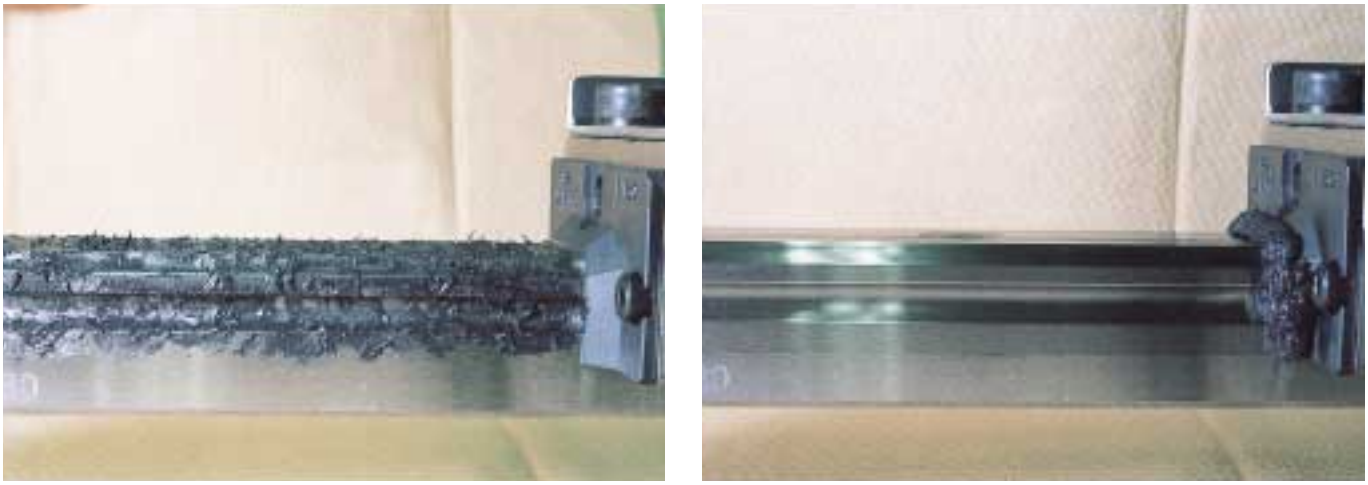

Before test

After test

Photo 2 Rail before and after test of high-performance side seal

Features

■ High sealing performance

For evaluation of the effectiveness of the new side seals, graphite particles 0.037 mm in average diameter were applied to the rail and side seals were moved back and forth along the rail by means of a test rig. The amount of graphite particles that remained on the rail after sliding the seals was measured. As shown in Fig. 2, the amount of particles left on the rail with the high-performance side seal was less than one-tenth of the single standard side seal. Photo 2 shows the rail surface before and after the high-performance side seal was tested.

■ Long Life

For evaluation of the endurance of linear guides with different side seals under heavy contamination, the linear guides were operated as fine wood powder was sprinkled on the rail. The ball slides were lubricated with grease before the test and were not replenished during the test.

Fig. 3 shows the test results. The linear guide fitted with the high-performance side seals exhibited a life more than twice as long as the linear guides fitted with standard side seals. Additionally, an endurance test performed under exposure to rubber powder showed more than 3.5 times longer life for linear guides with the new side seals.

Available Models and Dimensions

Currently available models of NSK linear guides with the new high-performance side seals are LH25, LH30, LH35 and LH45. Additional models will be developed in the future. Table 1 lists the dimensions of the ball slides available with high-performance side seals and NSK K1™ lubrication units. Also listed are the dimensions of ball

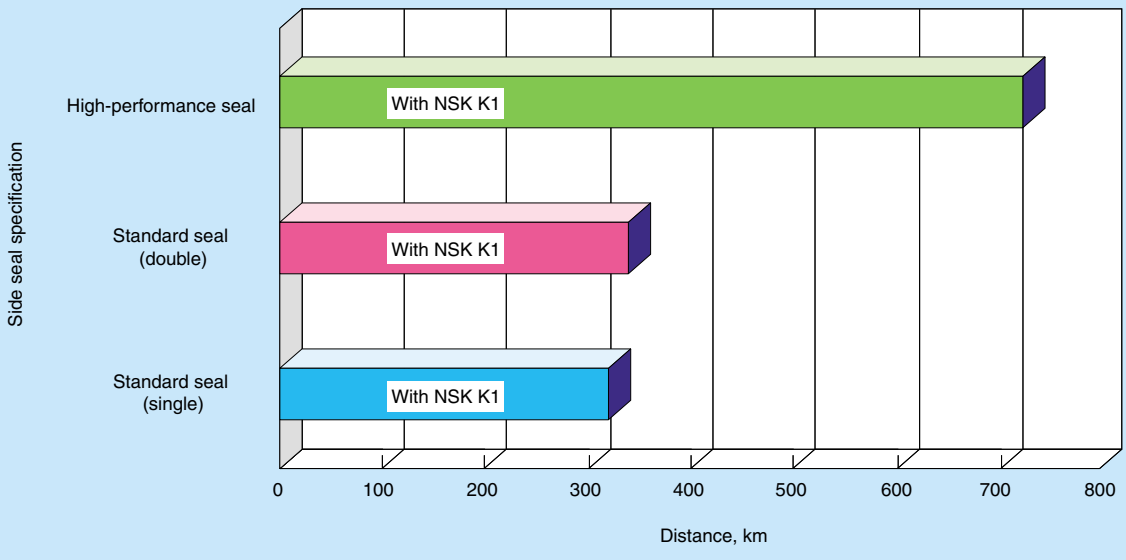

Fig. 3 Results of endurance tests under wood particle contamination

Table 1 Dimensions of ball slides fitted with high-performance side seals and NSK K1

Model		Ball slide length, *L*, mm	Nipple protrusion length *N*, mm
LH25	AN/EL/FL	97.0 (104.4)	8.0 (11.0)
	BN/GL/HL	125.0 (132.4)	
LH30	AN	104.4 (114.8)	7.0 (16.4)
	EL/FL	117.4 (127.8)	
	BN/GL/HL	143.4 (153.8)	
LH35	AN/EL/FL	128.8 (139.2)	7.0 (16.4)
	BN/GL/HL	162.8 (173.2)	
LH45	AN/EL/FL	161.4 (174.2)	8.5 (22.2)
	BN/GL/HL	193.4 (206.2)	

Note: The figures in parentheses are the lengths of the ball slides when fitted with seal protectors.

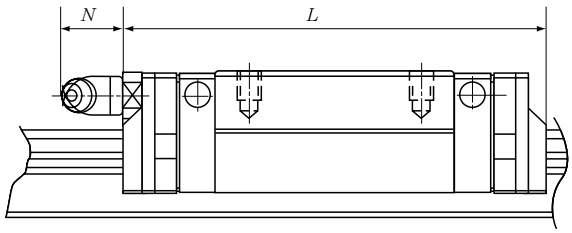

slides with side seal protectors that are attached to the outside of the seals.

Applications

NSK linear guides with high-performance side seals are especially suited for machines that are exposed to dust, powder and particles during operation, including:

- Woodworking machines
- Tire-buffing machines
- Welding lines
- Machines that work with graphite
- Laser cutting machines

Conclusion

Linear guides are increasingly used in environments contaminated by dust and other particulate matter. Working together with NSK K1™ lubrication units, new high-performance side seals are expected to be used extensively in such environments.

Notes:

Notes: